การจำลองซีเอฟดีแบบ 3 มิติ ของการสังเคราะห์สังกะสีออกไซด์ด้วยปฏิกิริยา
ในวัฏภาคก๊าซ

นางสาวภัสภรณ์ มหาผลศิริกุล

วิทยานิพนธ์นี้เป็นส่วนหนึ่งของการศึกษาตามหลักสูตรปริญญาวิศวกรรมศาสตรมหาบัณฑิต
สาขาวิชาวิศวกรรมเคมี ภาควิชาวิศวกรรมเคมี
คณะวิศวกรรมศาสตร์ จุฬาลงกรณ์มหาวิทยาลัย
ปีการศึกษา 2556
ลิขสิทธิ์ของจุฬาลงกรณ์มหาวิทยาลัย

THREE-DIMENSIONAL CFD SIMULATION OF ZINC OXIDE SYNTHESIS BY GAS-PHASE REACTION

Miss Passaporn Mahaphonsirigul

A Thesis Submitted in Partial Fulfillment of the Requirements

for the Degree of Master of Engineering Program in Chemical Engineering

Department of Chemical Engineering

Faculty of Engineering

Chulalongkorn University

Academic Year 2013

Thesis Title	THREE-DIMENSIONAL CFD SIMULATION OF ZINC OXIDE SYNTHESIS BY GAS-PHASE REACTION
By	Miss Passaporn Mahaphonsirigul
Field of Study	Chemical Engineering
Thesis Advisor	Associate Professor D.eng.Tawatchai Charinpanitkul
Thesis Co-Advisor	Ph.d.Pimporn Ponpesh

Accepted by the Faculty of Engineering, Chulalongkorn University in Partial Fulfillment of the Requirements for the Master's Degree

⋯⋯⋯⋯⋯⋯⋯⋯⋯⋯⋯⋯⋯⋯Dean of the Faculty of Engineering

(Professor Bundhit Eua-arporn, Ph.D.)

THESIS COMMITTEE

⋯⋯⋯⋯⋯⋯⋯⋯⋯⋯⋯⋯⋯⋯Chairman

(Associate Professor Artiwan Shotipruk, Ph.D)

⋯⋯⋯⋯⋯⋯⋯⋯⋯⋯⋯⋯⋯⋯Thesis Advisor

(Associate Professor Tawatchai Charinpanitkul, D.eng.)

⋯⋯⋯⋯⋯⋯⋯⋯⋯⋯⋯⋯⋯⋯Thesis Co-Advisor

(Pimporn Ponpesh, Ph.D.)

⋯⋯⋯⋯⋯⋯⋯⋯⋯⋯⋯⋯⋯⋯Examiner

(Assistant Professor Benjapon Chalermsinsuwan, Ph.D.)

⋯⋯⋯⋯⋯⋯⋯⋯⋯⋯⋯⋯⋯⋯External Examiner

(Santi Wattananusorn,Dr.-lng.)

ภัสภรณ์ มหาผลศิริกุล : การจำลองซีเอฟดีแบบ 3 มิติ ของการสังเคราะห์สังกะสี ออกไซด์ด้วยปฏิกิริยาในวัฏภาคก๊าซ. (THREE-DIMENSIONAL CFD SIMULATION OF ZINC OXIDE SYNTHESIS BY GAS-PHASE REACTION) อ.ที่ปรึกษาวิทยานิพนธ์หลัก: รศ. ดร.ธวัชชัย ชรินพาณิชกุล, อ.ที่ปรึกษาวิทยานิพนธ์ร่วม: ดร.พิมพ์พร พลเพชร, 74 หน้า.

ในวิทยานิพนธ์นี้ได้ใช้หลักการพลศาสตร์ของไหลเชิงคำนวณ(ซีเอฟดี) เพื่อศึกษา ผลกระทบของอุณหภูมิของการสังเคราะห์สังกะสีออกไซด์(ZnO)ด้วยปฏิกิริยาในวัฏภาคก๊าซ ภายในเครื่องปฏิกิริยาเคมีแบบท่อไหลช่วงของอุณหภูมิถูกศึกษาในช่วง 650องศาเซลเซียสถึง 1,200 องศาเซลเซียสในขณะที่การทดลองศึกษาอยู่ในช่วง 900องศาเซลเซียสถึง 1,000 องศา เซลเซียสทั้งนี้เนื่องจากข้อจำกัดของการทดลอง เช่น ต้นทุน เวลา วัสดุและ อุปกรณ์ จึงทำให้มี ข้อมูลเพียงจำกัดที่ศึกษาอิทธิพลของอุณหภูมิต่อผลได้ของสังกะสีออกไซด์ อีกทั้งหลักการซีเอฟดี เป็นเครื่องมือที่มีประสิทธิภาพซึ่งสามารถนำมาใช้ร่วมกับการทดลองเพื่อแก้ปัญหาและวิเคราะห์ ผลกระทบของอุณหภูมิที่ส่งผลกระทบต่อผลได้ของสังกะสีออกไซด์ ในการศึกษาได้พิจารณา สนามการไหลของก๊าซซึ่งถูกดิสครีไทเซชันภายในโดเมนทรงกระบอกสามมิติ จากนั้นจึงคำนวณค่า ผลได้ของสังกะสีออกไซด์ที่อุณหภูมิที่แตกต่างกันโดยใช้โปรแกรม FLUENT ในการศึกษาได้ทำ การยืนยันความถูกต้องของแบบจำลองที่สร้างขึ้น โดยนำผลจากการจำลองผลได้ของสังกะสี ออกไซด์มาเปรียบเทียบกับรายงานผลการทดลองก่อนหน้านี้ สำหรับผลกระทบของอุณหภูมิที่มีต่อ ผลได้ของสังกะสีออกไซด์ จากผลการจำลองพบว่าอุณหภูมิจะมีอิทธิพลสูงต่อผลได้ของสังกะสี ออกไซด์ในช่วงอุณหภูมิระหว่าง650องศาเซลเซียสถึง 1,100 องศาเซลเซียสและมีผลเพียงเล็กน้อย ต่อผลได้ของสังกะสีออกไซด์ที่อุณหภูมิสูงกว่า1,100 องศาเซลเซียส

ภาควิชา	วิศวกรรมเคมี	ลายมือชื่อนิสิต	
สาขาวิชา	วิศวกรรมเคมี	ลายมือชื่อ อ.ที่ปรึกษาวิทยานิพนธ์หลัก	
ปีการศึกษา	2556	ลายมือชื่อ อ.ที่ปรึกษาวิทยานิพนธ์ร่วม	

5470530521 : MAJOR CHEMICAL ENGINEERING

KEYWORDS: CFD SIMULATION / ZNO / TUBULAR REACTOR / GAS-PHASE REACTION

PASSAPORN MAHAPHONSIRIGUL: THREE-DIMENSIONAL CFD SIMULATION OF ZINC OXIDE SYNTHESIS BY GAS-PHASE REACTION. ADVISOR: ASSOC. PROF. TAWATCHAI CHARINPANITKUL, D.ENG. CO-ADVISOR: PIMPORN,PH.D. PONPESH, 74 pp.

In this thesis computational fluid dynamics (CFD) has been employed to examine effect of temperature on zinc oxide (ZnO) synthesisis gas-phase reaction within a tubular reactor. Under this investigation, the temperature range was between 650 °C and 1,200 °C, while the range employed in experiments was between 900 °C and 1,100 °C. So far only few studies have experimentally investigated the effect of of temperature on the ZnO yield due to the limitations, such as cost, time, material and equipment. Meanwhile, CFD is recognized as an effective tool for analysis of effect of temperature on ZnO synthesis yield. Gas flow field was discretized into a three-dimensional cylindrical domain. The yields of zinc oxide with different temperature were simulated using FLUENT® software. The developed models were validated by comparing the simulated yield of ZnO with the experimental data reported in some previous works.For the effect of temperature on yields of zinc oxide, the simulation results revealed that the temperature strongly affected the ZnO yields with the temperature range between 650 and 1,100 °C and slightly affected the yields with the temperature higher than 1,100 °C.

Department:	Chemical Engineering	Student's Signature ....
Field of Study:	Chemical Engineering	Advisor's Signature ....
Academic Year:	2013	Co-Advisor's Signature ....

ACKNOWLEDGEMENTS

CONTENTS

LIST OF TABLES

Table   **Page**

LIST OF FIGURES

Figure   **Page**

LIST OF ABBREVIATIONS

ALPHABETICAL SYMBOLS

E	Total energy
g	Gravitational force
J_i	Diffusion flux of species i
k	Thermal conductivity
k_0	Reaction rate constant
p	Pressure
R	Universal gas constant
Ri	Net rate of production of species i by chemical reaction
S_E	Energy source term
S_i	Species source term
S_{Mx}, S_{My}, S_{Mz}	Momentum source term in x,y,z directions

T   Temperature

t   Time

U   Velocity vector

u   x-velocity

v   y-velocity

w   z-velocity

Y_i Mass fraction of species i

GREEK SYMBOLS

μ   Viscosity

ρ   Fluid density

CHAPTER I

INTRODUCTION

1.1 Background and Motivation

Recently an interest in zinc oxide (ZnO) and its nanostructures has grown exponentially, as proved by an increasing number of ZnO-related literatures. ZnO is an oxide semiconductor with a wide direct band gap (3.3 eV) with high prospects in optoelectronics, especially because of its high excision binding energy (60 meV) [1]. Accordingly, ZnO is an important electronic and photonic material which could be used for UV light-emitters, gas sensors and acoustic wave devices. Recently, ZnO nanoparticles have attracted considerable attention due to their unique physical properties caused by the nanosized effect. Several studies have been conducted on their synthesis and structural property characterization. A number of methods are used for ZnO synthesis such as sol-gel, chemical vapor deposition and gas-phase reaction. Among these methods gas-phase reaction is advantageous because it can operate as a continuous process with high volume production and shorter amount of time. Lower unit cost, reduced need for apparatuses and energy savings can be achieved through automation and reduction of unnecessary labor. Besides, there is high yield and purity of the products. Moreover, gas-phase reaction was simple, low cost and reduced need for apparatuses [2]. However the investigation procedure of the influences from many

parameters is still not efficient enough due to the limitations of cost, time and technology. In this work focused on the ZnO synthesis using gas–phase reaction because this method widely used for simple operation and equipment which has made this method attractive for preliminary experimental trials carried out to study the behavior. In addition this method still lack of investigate about parameters that affect to yield of ZnO

Computational fluid dynamics simulation is a technical tool which uses numerical methods and algorithms to simulate and analyze problems that involve with fluid flow. The technique is very powerful and covers a wide range of industrial and non-industrial applications [3]. Some examples are fluidized bed combustion and gasification [4], industrial and environmental applications [5], heat exchangers design [6]. However, it is only in the recent decade that CFD has been applied to design and analysis of zinc oxide synthesis due to CFD is helping to generate cost saving in process. It give process of ZnO synthesis more complete understanding of the internal operation of reactor. The process of synthesis of zinc oxide investigation would be significantly enhanced if the integration of CFD and experiments is much developed. In particular, the design and reliability of experiments could be significantly enhanced by CFD [7]. This trend would be possible by the progress in CFD algorithms and the availability of ever more powerful affordable computers. It is well recognized that ZnO synthesis process involves complicated physical-chemical phenomena, such as

turbulence, oxidation, and so on. Mathematical modeling using CFD is an attractive method to help the understanding of hydrodynamics and heat transfer phenomena inside the reactor. In many cases, the investigations have been conducted in 2D because of lack of computer power.

CFD have a many application in 3D, for example particle suspension in a stirred tank [8], circulating fluidized bed boiler [9] and bubble column reactors [10]. Generally, results from 3D simulations do show an improvement in accuracy. Although 3D system consumes resources and time more than 2D system, the benefits of using CFD in 3D of various applications have already been used while zinc oxide synthesis emptying processes have not yet been studied in terms of CFD simulations in 3D.

At the present time due to the experimental limitation of ZnO synthesis such as cost, time, material and equipment, the combining of CFD simulation with experiment allows understanding phenomena occured in the reactor and enhancing effective to synthesize ZnO.

The objective of this study was to employ CFD simulation technique to investigate the effect of operating nitrogen flow rate and temperature on the yield of ZnO synthesis by gas-phase reaction

1.2 Objectives of the Research

To employ CFD simulation technique to investigate effect of operating temperature and nitrogen gas flow rate on zinc oxide synthesis using gas-phase reaction

1.3 Scope of the Research

1.3.1   Conduct survey to collect data of model of zinc oxide synthesis using gas phase reaction

1.3.2   Develop a suitable 3D and 2D CFD model to study fluid flow phenomena of zinc oxide synthesis using gas phase reaction

1.3.3   Validate model for zinc oxide synthesis using gas phase reaction and compare the results between 3D and 2D

1.3.4   Employ validated 3D model to investigate the effect of Gas flow rate and temperature on zinc oxide synthesis out of the range employed in previous experiments

- Effect of temperature between 650 °C and 1,200 °C

- Effect of nitrogen flow rate between 0.05 lit/min and 4 lit/mi

- CHAPTER II

- THEORY AND LITERATURE REVIEW

-

2.1 Zinc oxide

    2.1.1 Properties of zinc oxide

Zinc oxide is an inorganic compound with the formula ZnO. ZnO is a white

powder shows in Figure 2.1. It is widely used as an additive in numerous materials and

products and is insoluble in water. The ZnO structures are hexagonal which is shown

in Figure 2.2. In materials science, ZnO is a wide-bandgap of the II-VI semiconductor

group at room temperature and a large free-exciton binding energy. The typical

properties of zinc oxide are shown in the Table2.1.

-     Figure2.1 Zinc Oxide powders
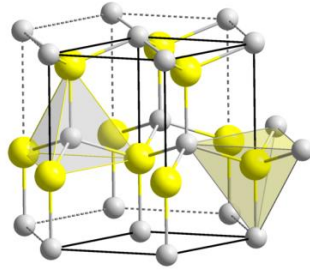
Figure2.2 Zinc Oxide Structure

Table2.1 Typical properties of zinc oxide

Properties	Value
Band Gap Energy	3.3 eV
Exciton binding Energy	60 meV
Molecular weight	81.38
Density	5.67 g/cm^3
Melting point	1975℃
Thermal conductivity	130 W/m.K

2.2 Synthesis of zinc oxide

Several approaches are presently being investigated to synthesize ZnO nanopowders, such as chemical vapor deposition [1], hydrothermal treatment [2], and gas-phase reaction [3]. From alternative several techniques, gas-phase reaction has

enjoyed increasing interest because of the following advantages i) gas-phase reaction can usually be better controlled because of the convenient way in which the reactants are supplied and mixed ii) the composition of the environment is better controlled so that contamination is reduce, iii) rate of reaction and react mechanism are conveniently controlled by the temperature of the substrate and of the reacting gases [4] Usually, commercial ZnO particles could be synthesized by two methods as following.

2.2.1 French process

Metallic zinc is melted in a graphite crucible and vaporized at temperatures above 907 ℃. Zinc vapor reacts with the oxygen in the air to give ZnO, accompanied by a drop in its temperature and bright luminescence. Zinc oxide particles are transported into a cooling duct and collected in a bag house. This indirect method was popularized by LeClaire (France) in 1844 and therefore is commonly known as the French process. Its product normally consists of agglomerated zinc oxide particles with an average size of 0.1 to a few micrometers. By weight, most of the world's zinc oxide is manufactured via French process [5].

2.2.2 American process

An American process for zinc oxide production from oxidized ore was developed in 1851. American- process zinc oxide, also is commonly called "direct ZnO", result from the reduction by coal, and the products of partial combustion, particularly carbon monoxide, of oxidized zinciferous materials to produce zinc vapour.

The zinc vapour is subsequently oxidized. In the early stages, raw materials were zinc

ores or roasted zinc sulfide. Nowadays the industry mostly uses technical grade oxides

obtained from fine fraction of brass ashes. American process zinc oxides are particularly

well suited for paint, ceramic and rubber industry[6].

2.2.3 ZnO synthesizing reaction

Chemical reactions of the ZnO synthesis is the heart of process, making

possible the achievement of its ultimate goals, which include synthesizing materials

with desired properties. Ordinary reaction of zinc oxide synthesis using Gas-phase

reaction to be form [7]

$$Zn + \frac{1}{2}O_2 \rightarrow ZnO$$
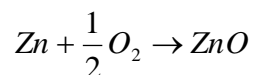
The global reaction rate can be described as follows:

$$-\frac{d[Zn]}{dt} = k_0 \exp\left(\frac{-E_a}{RT}\right)[Zn][O_2]^{1/2} \tag{1}$$

Here [Zn] is the reactant concentration, [O_2] the oxidant concentration, t the reactor

residence time. Ea, k and k_0 represent the activation energy, reaction rate constant

and the Arrhenius constant specific for the reaction, respectively

$$-r_{Zn} = r_{ZnO} = k[Zn][o_2]^{\frac{1}{2}} \tag{2}$$

Reuge et al.(2009) employed Eq. (1) for the CFD simulation of ZnO particle formation in parallel flow and cross flow reactor[8]. They adopted the activation energy reported by Garcia et al.(2005) and determined the frequency factor as:

$$k_0 = 8 \times 10^{-8} \exp\left(-\frac{12.9 \times 10^7}{RT}\right)$$

Since the change in the oxidant concentration throughout the reaction was assumed insignificant because of the excess oxygen concentration, the global reaction rate can be considered to be a pseudo-first-order reaction with respect to the Zn concentration, assuming a zero order for oxygen concentration [21]

2.3 Computational Fluid Dynamics (CFD)

Computational fluid dynamics, usually abbreviated as CFD, is a branch of fluid mechanics that uses numerical methods and algorithms to solve and analyze problems that involve fluid flows, heat transfer and associated phenomena such as chemical reactions by means of computer-based simulation. Flows and related phenomena can be described by partial differential equation. To obtain an approximately differential equations by a system of algebraic equations, which can be solved on a computer. The approximates are applied to small domains in space and time so the numerical solution provides results at discrete locations in space and time [9].

2.3.1 CFD processing

In general, CFD contains three main elements which represent as the follows:

Pre-processor [10]

All the tasks that take place before the numerical solution process are called pre-processing. This includes

- Definition of the geometry of the region of interest

- Mesh of calculation domain and generation of a computational model

- Selection of the physical and chemical phenomena that need to be modeled

- Definition of fluid properties, Specification of appropriate boundary conditions

Solver

Processing involves using a computer to solve mathematical equations of fluid flow. Once the meshing is completed, the model input values should be specified and then the software can solve the equations of state for each cell until an acceptable convergence is achieved. This is a very intensive process and usually it requires the computer to solve many thousands of equations. In each case, the equations are integrated and the boundary conditions are applied to it. This is known as equation discretisation and applied to each individual cell of the mesh. The process is repeated

in an iterative manner until a required accuracy is achieved. This step can be a time-consuming process and although it is the core of any CFD software package, little of its operation can be seen.

Post-processor

The post-processing program is used to make evaluation of the data generated by the CFD analysis. When the model has been solved, the results can be analyzed both numerically and graphically. Post-processing tools of the powerful CFD software can create visualisation ranging from simple 2-D graphs to 3-D representations. Typical graphs obtained with the post-processor might contain a section of the mesh together with vector plots of the velocity field or contour plots of scalar variables such as pressure. In such graphs, colors are used to differentiate between the different size of the values.

CFD processing can be summarized as a diagram, shown in Figure 2.1.
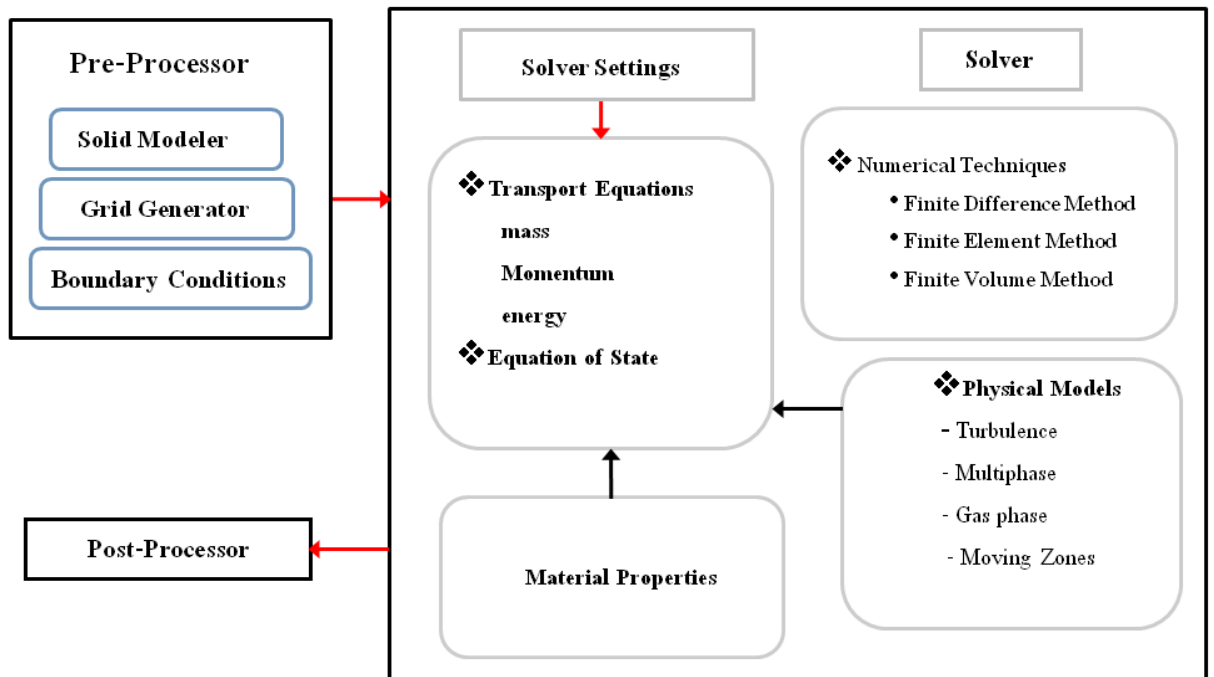
Figure2.3 CFD processing diagram

2. 4 Single phase solver option[11]

In this work CFD simulation of ZnO synthesis operated as a homogeneous gas phase so that single phase setting is important to use for model accuracy. Two main general specifications were applied for overall problem. The solver was considered to be a Pressure-Based solver which used the Navier-Stokes equations of continuity to determine velocities based on pressure because only information on inlet velocities and outlet pressure were supplied.

The material for the single phase simulation was gas phase. Eliptic Boundary Conditions were required, and these included supplying an inlet mass flow rate being placed on the whole system. The Solution methods and Controls were kept default

for single phase flow. By selecting specific monitors, the pressure could be monitored during solving which helped to avoid premature convergence. Premature convergence was also avoided by changing the residual constraints. Defining the number of iterations under Controls made it possible to observe the trends in pressure and pressure drop during the calculation of a solution, which helped to ensure that a more viable end result was achieved.

2.5 Governing equations

The derivation of the principle equations of fluid dynamics is based on the fact that the dynamical behavior of a fluid is determined by the following:

2.5.1 Mass conservation equation or Continuity equation

In order to derive the continuity equation, consider the model of a finite control volume fixed in space, as sketched in Fig. 2.4. At a point on the control surface, the flow velocity vector is u the unit normal vector is $\vec{n}$ and dS denotes an elemental surface area. The conserved quantity in this case is the density designated by ρ. Body forces caused by gravity $\mathbf{g}$ and acceleration $\mathbf{a}$ act on the center of mass of the control volume. For the time rate of change of the total mass inside the finite volume v
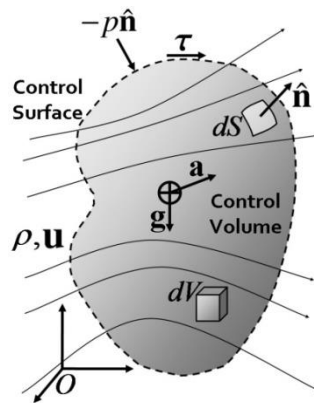
Figure2.4 control volume

The flow velocity of fluid is defined as $U = u_i + v_j + w_k$. The unsteady mass conservation equation or continuity equation of compressible fluid may be written as

$$\frac{\partial \rho}{\partial t} + \frac{\partial}{\partial x}(\rho u) + \frac{\partial}{\partial y}(\rho v) + \frac{\partial}{\partial z}(\rho w) = 0 \qquad (3)$$

or

$$\frac{\partial \rho}{\partial t} + \nabla \cdot (\rho \mathbf{U}) = 0 \qquad (4)$$

For an incompressible fluid the density (ρ) is constant and continuity equation becomes

$$\nabla \cdot \mathbf{U} = 0 \qquad (5)$$

Species transport equation

$$\frac{\partial \rho Y_i}{\partial t} + \nabla \cdot (u \rho Y_i) = \nabla \cdot (\partial J) + S_{i_i} + R_i \tag{6}$$

2.5.2 Momentum equation

The derivation of the momentum equation by recalling the particular form of Newton's second law which states that the variation of momentum is caused by the net force acting on a mass element for the momentum of an infinitesimally small portion of the control volume (see Fig. 2.4)

The momentum equation for a Newtonian fluid may be written as

x-component

$$\rho \frac{Du}{Dt} = -\frac{\partial p}{\partial x} + \frac{\partial \tau_{xx}}{\partial x} + \frac{\partial \tau_{yx}}{\partial y} + \frac{\partial \tau_{zx}}{\partial z} + S_{Mx} \tag{7}$$

y-component

$$\rho \frac{Dv}{Dt} = -\frac{\partial p}{\partial y} + \frac{\partial \tau_{xy}}{\partial x} + \frac{\partial \tau_{yy}}{\partial y} + \frac{\partial \tau_{zy}}{\partial z} + S_{My} \tag{8}$$

z-component

$$\rho \frac{Dw}{Dt} = -\frac{\partial p}{\partial z} + \frac{\partial \tau_{xz}}{\partial x} + \frac{\partial \tau_{yz}}{\partial y} + \frac{\partial \tau_{zz}}{\partial z} + S_{Mz} \tag{9}$$

Here, S_M is the momentum source term, and p is pressure gradient

viscous stress of fluid are denoted by τ.

2.5.3 Energy equation

The first law of thermodynamics is applied in the derivation of the energy

equation. Applied to the control volume displayed in Fig.2.4, it states that any changes

in time of the total energy inside the volume are caused by the rate of work of forces

acting on the volume and by the net heat flux into it. The energy equation becomes

(10)

$$\rho \frac{DE}{Dt} = \frac{\partial(up)}{\partial x} - \frac{\partial(wp)}{\partial y} + \frac{\partial}{\partial x}k\left(\frac{\partial T}{\partial x}\right) + \frac{\partial}{\partial y}k\left(\frac{\partial T}{\partial y}\right) + \frac{\partial}{\partial z}k\left(\frac{\partial T}{\partial z}\right)$$

$$+ \frac{\partial(u\tau_{xx})}{\partial x} + \frac{\partial(u\tau_{yx})}{\partial y} + \frac{\partial(u\tau_{zx})}{\partial z} + \frac{\partial(v\tau_{xy})}{\partial x} + \frac{\partial(v\tau_{yy})}{\partial y} + \frac{\partial(v\tau_{zy})}{\partial z}$$

$$+ \frac{\partial(w\tau_{xz})}{\partial x} + \frac{\partial(w\tau_{yz})}{\partial y} + \frac{\partial(w\tau_{zz})}{\partial z} + S_E$$

The specific energy (E) is defined as the sum of internal (thermal) energy,

kinetic energy and potential energy. The property k is thermal conductivity and S_E is

energy source term.

2.5.4 General transport equations [23]

There are significant commonalities among equations (5), (6), (7), (8), (9) and (10). If we introduce a general variable Φ the conservative form of all fluid flow equations, including equations for scalar quantities, such as temperature and concentration etc., can usefully be written in the following form

$$\frac{\partial(\rho\Phi)}{\partial t} + \nabla.(\rho\Phi u) = \nabla.(\Gamma\nabla.\Phi) + S_{\Phi} \qquad (11)$$

The rate of change term and the convective term on the left hand side and the diffusive term (Γ =diffusion coefficient) and the source term respectively on the right hand side. Equation 8 is used as the starting point for computational procedures in the finite volume method. By setting Φ equal to 1, *u*, *v*, *w* and *i* and selecting appropriate values for Γ (diffusion coefficient) and source terms, we obtain special forms for each of the five PDEs for mass, momentum and energy conservation. The key step of the finite volume method is the integration of equation 10 over a three-dimensional control volume (CV)

2.6 Finite volume method [1]

The finite volume method (FVM) is a discretization technique for partial differential equations, especially those that arise from physical conservation laws. FVM is in common use for discretizing computational fluid dynamics equations.

The steady convection–diffusion equation can be derived from the transport equation for a general property Φ by deleting the transient term, the following form:

$$\nabla.(\rho\Phi u) = \nabla.(\Gamma\nabla.\Phi) + S_{\Phi}$$

The control volume integration, which forms the key step of the finite volume method that distinguishes it from all other CFD techniques, the following form:

$$\int_{cv}\nabla.(\rho\Phi u)dv = \int_{cv}\nabla.(\Gamma\nabla.\Phi)dv + \int_{cv}S_{\Phi}dv$$

This equation represents the flux balance in a control volume. The left hand side gives the net convective flux and the right hand side contains the net diffusive flux and the generation or destruction of the property Φ within the control volume

Finite volume method consists of the following steps

Grid generation

The first step in the finite volume method is to divide the domain into discrete control volumes

Discretisation

The meshing of the computational domain substitutes the continuous domain with the partial differential equations describing the flow, by a discrete problem with finite number of volumes (meshes) where the flow is described by differential equations. In general the discretisation procedures use structured (rectangles or parallelepipeds) or unstructured (triangles or tetrahedra) meshing. In this study structured meshing was used in order to represent the fluid stream of ZnO synthesis in the tubular reactor and to ensure a good numerical stability [12].

Solution of equations

Discretised equations must be set up at each of the nodal points in order to solve a problem. The resulting system of linear algebraic equations is then solved to obtain the distribution of the property Φ at nodal points

2.7 Literature Reviews

2.7.1 Investigation on synthesis of zinc oxide

Charinpanitkul et al. [13] synthesized ZnO nanoparticles using a modified French process in which oxygen and nitrogen flow rates were controlled. ZnO nanoparticles synthesized with the lower O2/N2 feed ratio exhibited the uniform tetrapodal nanostructure with high crystallinity. The increase in the O2 supply would lead to further growth of tetrapodal ZnO nanoparticles. However, the excessive N2 flow would lead to the shorter residence time of reactive zinc vapor exhibit the interstitial surface-bound zinc, which preferably enhance the blue PL emitting characteristics

Charnhattakorn et al. [14] synthesized zinc oxide nanoparticles by the French process modified with pulsed injection of nitrogen. Nitrogen pulse increases the reaction between zinc vapor and oxygen in the French process and control oxygen vacancies within zinc oxide nanocrystals. Characteristics of the pulse, i.e. flowing and non-flowing period of the gas, pulsing cycle time, and the supplied pressure of the injected gas influence on the content of oxygen vacancies. The longer nitrogen pulse could provide higher growth of tetrapod zinc oxide with higher oxygen vacancies.

Hsu et al. [15] investigated the influence of zinc and oxygen supply on the morphology and optical properties of zinc nanostructures which were synthesized by gas phase reaction. Zinc and oxygen supply are converted by oxygen gas flow rate and

the amount of zinc source material under zinc-rich conditions, large diameter changes from microwhiskers to nanoneeedles are observed, while the samples exhibited strong green defect emission. Under oxygen-rich conditions, smaller diameter variations are found, and the emission spectrum is dominated by the UV instead of defect emission. Moreover, high UV-to-defect emission ratio is obtained from optimal amount of zinc supply, and further increase in zinc supply resulted in increase of the defect emission.

Shen et al. [16] researched the influences of Zn vapor, oxidization time and temperature in order to control morphologies of tetrapod ZnO nanocrystals. The process was separated to be evaporation zone and condensation zone. Tetrapod ZnO depended on variation of ZnO condensation temperature and time. ZnO tetrapod legs were synthesized dividing to two types. The first one is uniform hexagonal. The second one is hierarchical hexagonal. The ZnO vapor was completely formed in thicker part of leg. The leg morphology of the tetrapod ZnO depended on Zn vapor oxidization temperature and time. The increase of the thermostatic ZnO condensation time resulted in the morphology transition of the tetrapod legs from hierarchical hexagonal (HH) to uniform hexagonal (UH) prism. At higher condensation temperature and longer condensation time resulted to tetrapod ZnO nanocrystals with uniform hexagonal (UH) legs.

2.7.2 Synthesis of zinc oxide using the combination of experiments and

Computational Fluid Dynamics (CFD)

Reuge et al. [17] studied the synthesis of zinc oxide tetrapods from zinc metal

by using a combination of experiments and computational fluid dynamics. The

commercial CFD code of this research is FLUENT which based on Finite Volume

Method (FVM). The experimental study allowed ultrapure zinc oxide particles with 250-

450 nm of mean lengths and 14-27 nm of mean diameters. Configuration (i.e. parallel

flow/cross flow) affected on Zinc oxide nanorods, but the position of air injection was

not affected. However, the yield of the reaction depended both on the reactor

configurations and on the position of air injection. The combination of the

experimental and simulated results led to better understanding of heat and mass

transfer. Cross flow configurations gave maximum yield for all tested conditions. For

the several parameters, such as argon and air flow rates, position of air injection, etc.,

were varied in the simulation to find the optimized reaction conditions for maximum

yield and production rate. For cross flow configuration, the simulation results showed

71% yield and a production rate 7 times higher than the nominal value that had been

obtained.

Yamamoto et al. [18] generated tetrapod zinc oxide nanoparticles via gas-

phase reaction of Zn vapor and oxygen in air with using flow restrictor. In case flow

restrictor, the leaving sufficient amounts of unreacted Zn vapor formed tetrapod zinc

oxide. Phenomena inside the reactor were analyzed by computational fluid dynamics. The simulated results showed the flow restrictor suppresses the mixing and reduced the residence time in the reactor, so the remaining unreacted Zn vapor allowed the zinc oxide particles to grow in tetrapod-shape.

2.7.3 CFD with 3D simulation

Ekambara et al. [19] studied flow pattern in bubble column reactors using 1D, 2D and 3D $k-\epsilon$ models by using CFD tecqhnique. All the models showed good conform with the experimental data for axial liquid velocity and the fractional gas hold-up profiles. However, as regards to eddy diffusivity, only the 3-D model predictions agreed closely with the experimental data. The 1-D, 2-D simulations overpredicted the values by 20–100% and 50–200%, respectively.

Moroz et al. [20] used intensively 3D simulation in turbine flow path and its components design. At the same time, whereas unidimensional and axisymmetric analyses are mostly used in the industry practice. CFD solver tested the data that obtained from experiments conducted on a single stage air turbine model with the results of 1D and 2D modeling and 3D simulation for comparision. The results were analyzed to validate a judgment of the authors that along with 3D CFD methods.

The experiment of ZnO synthesis have a many restriction such as, cost, time, equipments and materials. Therefore, some additional tool were needed to be help for increase effectiveness of process. CFD is a one potential tool for investigation to help understanding of hydrodynamics and heat transfer phenomena inside the reactor. At the present, many work still investigated about 2D CFD simulation of ZnO but 3D simulation have not been investigate. Some previous work lack of species mass reaction result to the model incomplete enough. This work focused on 3D simulation for improved the model of ZnO synthesis using gas-phase reaction
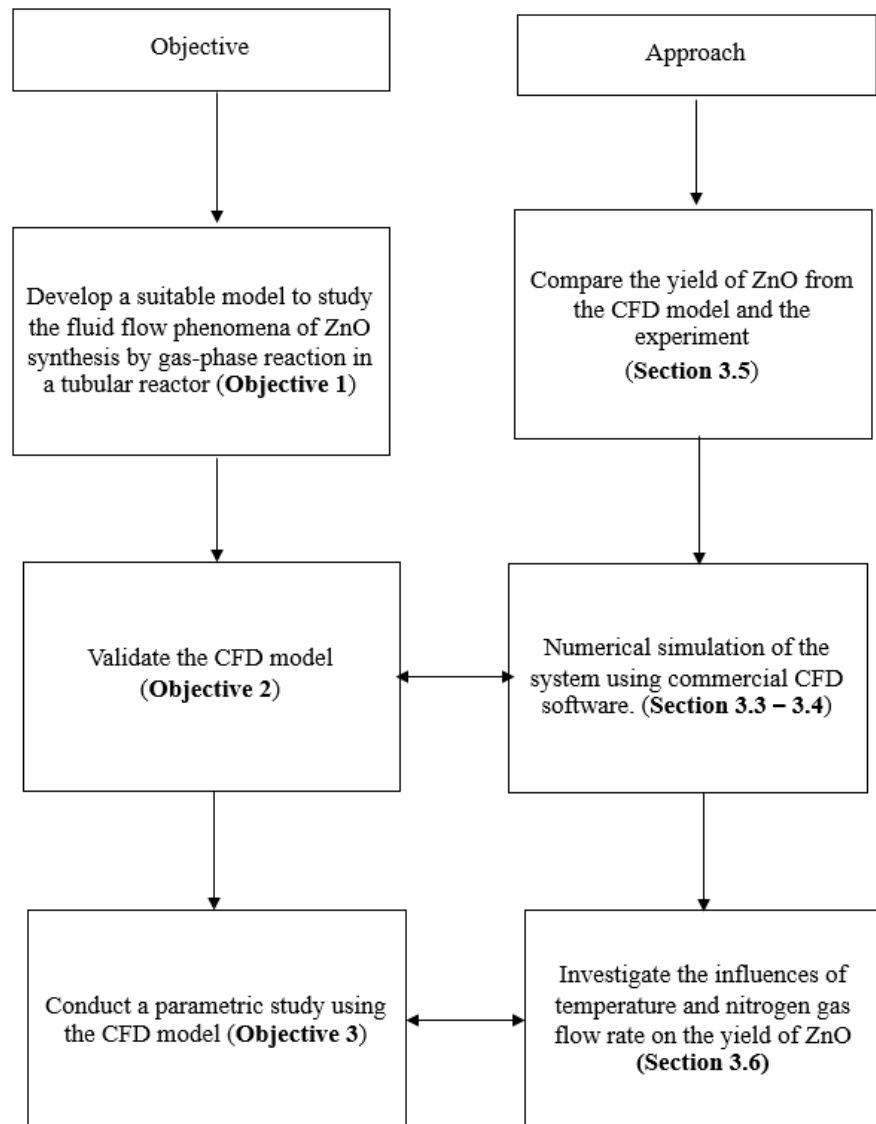
CHAPTER III

EXPERIMENTAL AND SIMULATION

Objective 1 concerned with develop a suitable model to study the fluid flow phenomena of ZnO synthesis by gas-phase reaction in a tubular reactor. The modelling of ZnO synthesis by using gas-phase reaction is a complicated task, due to the complexity of geometry and chemical phenomena. The challenge presented in this thesis was to choose a computational fluid dynamics (CFD) program which to simulate the experimental setup of zinc oxide synthesis by gas-phase reaction

Objective 2 reported the results for the simulations done to validate the models proposed by compare the simulated results yield of ZnO against the experimental results

Objective 3 used the results from the simulation to analyse the effect of the temperature and nitrogen flow rate to affect of ZnO yields. And then examine the effect of temperature and nitrogen flow rate which affect ZnO yields. Figure 3.1 illustrates the approaches to achieve the specific objectives in this study

Figure3.1 Flow diagram of objectives and related approaches

3.1 Material

Zinc dross was supplied by Foseco (Thailand) Co.Ltd as shown in Figure 3.2.

raw material. The purity of Zinc in zinc dross is 99.999%. Figure 3.3 shows ZnO which

was synthesized by gas phase reaction. The Zn particles were evaporated at 800 ℃.

Nitrogen were used in the reaction as a carrier gas. Nitrogen gases and nitrogen-oxygen

mixture were controlled flow rate at 2.0 l/min and 0.1325 l/min respectively .

.

Figure3.2 zinc dross supplied by FOSECO (Thailand)

Figure3.3 ZnO

3.2 Experimental procedure. [21]

ZnO particle were fabricated in a horizontal quartz tube furnace by gas phase reaction without catalyst. The quartz tube reactor was 120 cm in length 5.2 cm in diameter, and a porous ceramic tube, used as the inner tube, was with a length of 60 cm and a diameter of 3.6 cm. The electrical furnace was 30 cm in length. The Zn particle 4 g was loaded onto alumina boat in porous ceramic. Nitrogen was used as carrier gas. Then flow of nitrogen and oxygen gas mixture was used as reactant at 0.1325 l/min at the temperature of reaction from 920 °C. When the reactor was heated until 800 °C by the first electrical furnace the boat was moved into the reactor. The temperature for reaction was controlled by the second electrical furnace. After the growth process, the furnaces were allowed to cool down to ambient temperature. The ZnO particles deposited on quartz tube. After that the ZnO particle were characterized by scanning electronmicroscope (SEM).

3.3 Model setup

3.3.1 Modeling of zinc oxide reactor

The computational geometry of the tubular reactor was set up based on the experiments but choose the interesting region for model setup as shown in red frame in Fig. 3.4. The reactor consisted of a quartz tube, which was used as the outer tube, with a length of 30 cm and a diameter of 4.6 cm, and a porous ceramic tube, used as the inner tube, with a length of 5 cm and a diameter 3.6 cm. The reactor was equipped

with an axial tube at the upstream of the reactor for the delivery of air feed in quartz

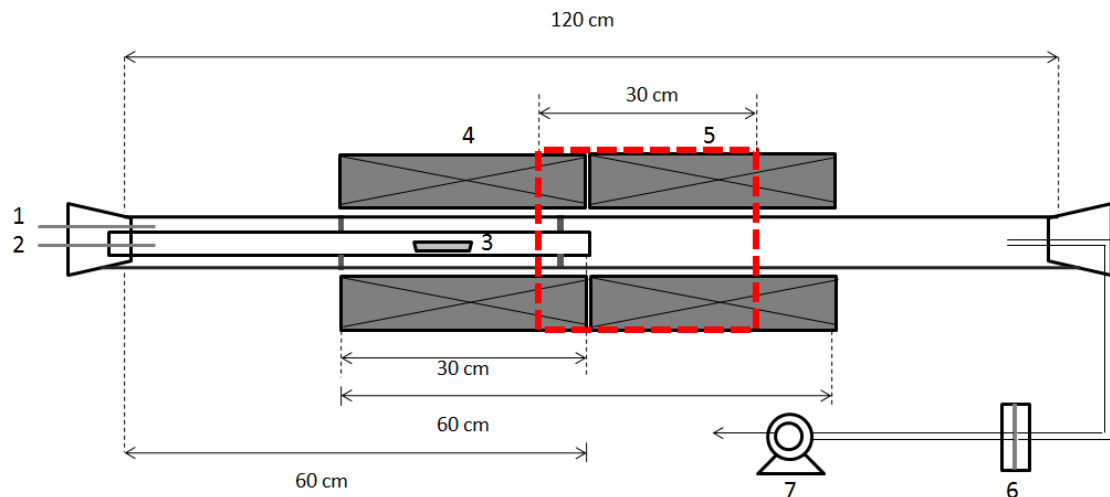tube and nitrogen carrier gas in porous ceramic tube to the reactor.

Figure3.4 Schematic diagram of experimental set-up (1) O_2/ N_2 mixture feed, (2) N_2 feed, (3) zinc powder loaded in aluminum boat, (4) electrical furnace for evaporation zone, (5) electrical furnace for reaction zone, (6) filter for particles collectors

(7) vacuum pump

A drawing of the computational physical domain considered to be two-

dimensional and three-dimensional, as shown in Figure 3.5 and Figure 3.6 respectively.

The first step of simulation was to generat the grids or cells, the model-geometry was

divided into discrete control volume, That was the most important step after the

definition of the domain geometry. The calculation domain and grid generation for

two-dimensional and three-dimensional geometry was done by GAMBIT, as shown in

Figure 3.7 and Figure 3.8 respectively. The quad mesh elements were used for the

simulation. In addition, very fine meshes were applied in the area of rapid changes of

the reaction rates. The 2D configuration (case (a)) required about 24,890 cells and the
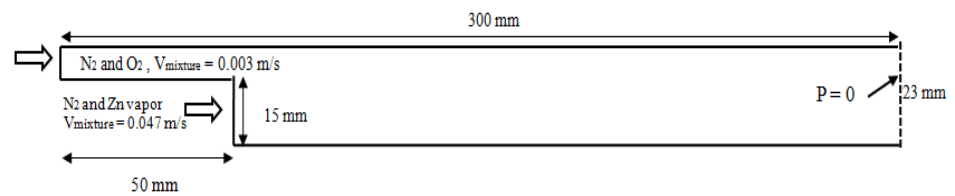
3D configuration (case (b)) more than 200,000 cells.

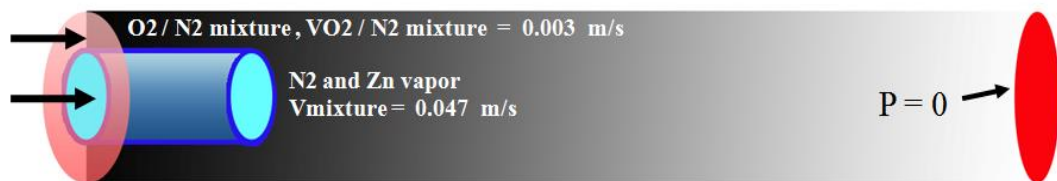*Figure3.5 2-D Simulation domain and its boundary condition*

Figure3.6 3-D Simulation domain and its boundary condition

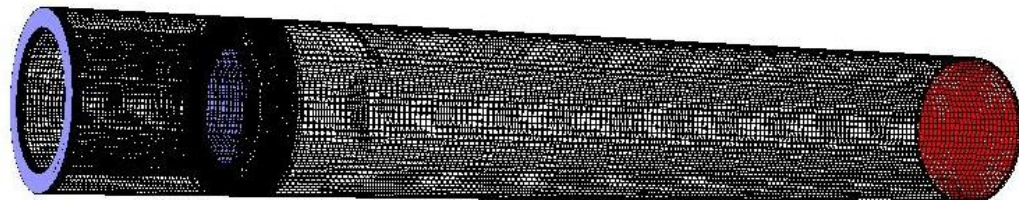Figure3.7 Gird generation in 2-D simulation domain

Figure3.8 Gird generation in 3-D simulation domain

3.3.2 Boundary conditions

The boundary conditions of this simulation for the two–dimensional CFD models and three–dimensional CFD models were set similar to the experimental. The reactor inlet boundary condition was assumed as a velocity inlet and the outlet boundary condition was specified as a pressure outlet with zero gauge pressure. In addition, the temperature variation inside the along tube of reactor was operated with a user-defined functions (UDF) as shown in appendix A. The inlet gas velocities are shown in Table 3.1.

Table3.1Inlet gas velocities

Feed	Velocity, (m/s)
Air	0.003
Nitrogen and Zn vapor	0.047

3.3.3 Assumptions of the model

The flow was considered to be incompressible ideal gas. The homogeneous gas phase reaction was only considered. Furthermore, when the velocity was 0.003 m/s, the Reynolds numbers was about 96. This indicated that the flow in the reactor was laminar. The governing equations were solved iteratively by using FLUENT, which base on the Finite Volume Method (FVM). The coupling of pressure and velocity were solved by using SIMPLE algorithm [22]. Second order upwind scheme was applied to calculate momentum, energy, and gas species.

3.4 Investigation of grid independence solutions

Grid-independenc means calculate results change so little along with a denser or looser grid that the truncation error can be ignored in numerical simulation. The grid is independent directly influences the truncation error and opearating time of numerical results. The previous research reveals that the grid resolution have a very great effect on the results of numerical simulation in a certain range [23]. Grid independent is the term used to describe the improvement of results by using successively smaller cell sizes for the calculations. A calculation should approach the correct answer as the mesh becomes finer, hence the term grid independent. The normal CFD technique is to start with a coarse mesh and gradually refine it until the changes observed in the results are smaller than a pre-defined acceptable error. In this work grid independent was carried out to investigate the effect of grid resolution on

the the prediction of CFD simulation of the transport phenomena inside the tubular reactor [24]

3.5 Validation of the model

Model validation is methodology for the development of computational ZnO synthesis using gas-phase reaction model that can be used to predicted yield of ZnO for reduce the time, cost, and risk associated with experimental of ZnO synthesis. The ZnO nanoparticle synthesis using gas-phase reaction in a tubular reactor was simulated using CFD technique. The species mass transport equations with laminar finite reaction rate were employed to calculate total mass of ZnO. The calculation procedure is shown in Fig 3.9. The simulation results of three different temperature, including 920°C, 950°C, and 1100°C, were validated by comparing with the experimental results. The boundary conditions (i.e., mass flow rate, temperature and mass fraction) in all simulations were setup corresponding to those in the experiments
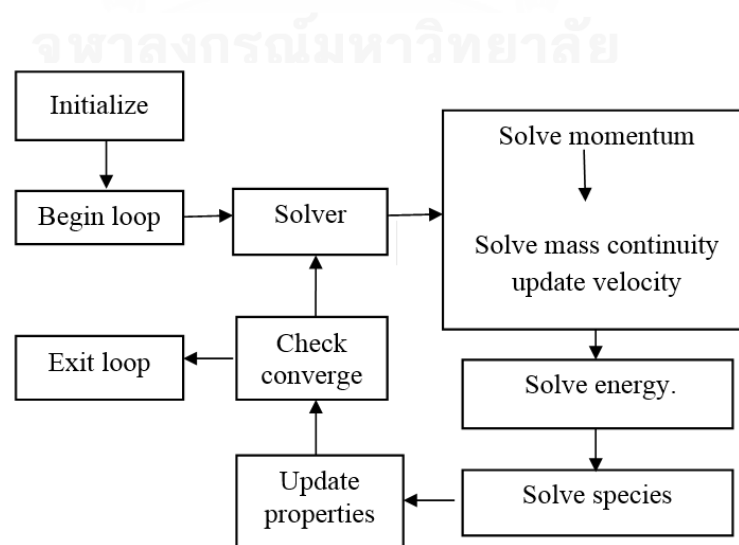

Figure3 9 Flowchart Fluent solver algorithms

3.6 Simulation of synthesis parameters which affect the yield of zinc oxide

The effect of N_2 flow rate and temperature were investigated out of the range employed in previous experiments. The investigation of this simulation was separated into two parts as follow.

3.6.1 Effect of nitrogen feed on zinc oxide yield

In this part, the effect of different nitrogen flow rate on ZnO yields was investigated by varying N2 flow rate between 0.05 lit/min and 4 lit/min

3.6.2 Effect of temperature on zinc oxide yield

In this part, the effect of reaction temperature on ZnO yields was investigated at the temperature range of 650 ℃ – 1200 ℃, including temperature which was the same value as that in the validation cas

CHAPTER IV

RESULTS AND DISCUSSION

4.1 Investigation of grid independent solutions

In this part, the reactor with was only modeled to examine grid independent solutions. All models were done by GAMBIT. The geometry of 2D and 3D were separated into two parts, including upstream zone and reaction zone as shown in Figure 4.1 and Figure 4.2. Grid generation of all models was controlled to be quad cell and very dense in the region of the rapid change. The grid generated at different grid resolutions as shown in Figure 4.3 and Figure 4.4. The goal is to obtain a grid-independent solution so that the models can be evaluated. The changes in the yields of ZnO at the grid resolution is in good agreement with experimental results. The results were converged by looking at residual values. It must be ensure that the solution is also independent of the mesh resolution, so that the next time a similar problem can apply the same mesh sizing. The normal CFD technique is to start with a coarse mesh and gradually refine it until the changes observed in the results are smaller than a pre-defined acceptable error
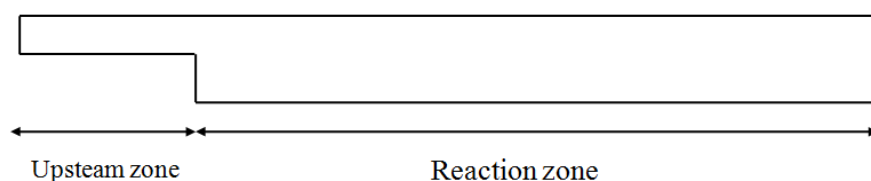

Upsteam zone   Reaction zone
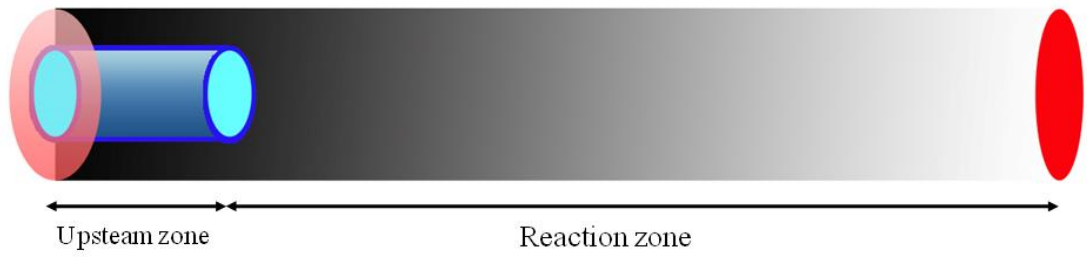
Figure4.1 Geometry of the model for two-dimension
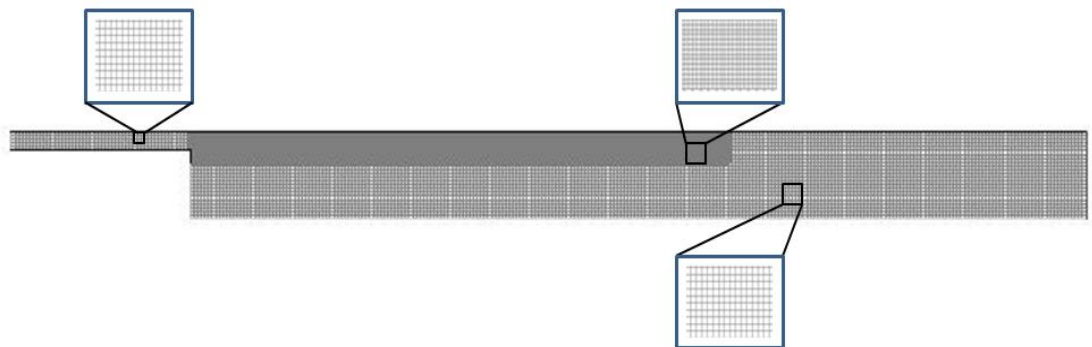
Figure4.2 Geometry of the model for three-dimension

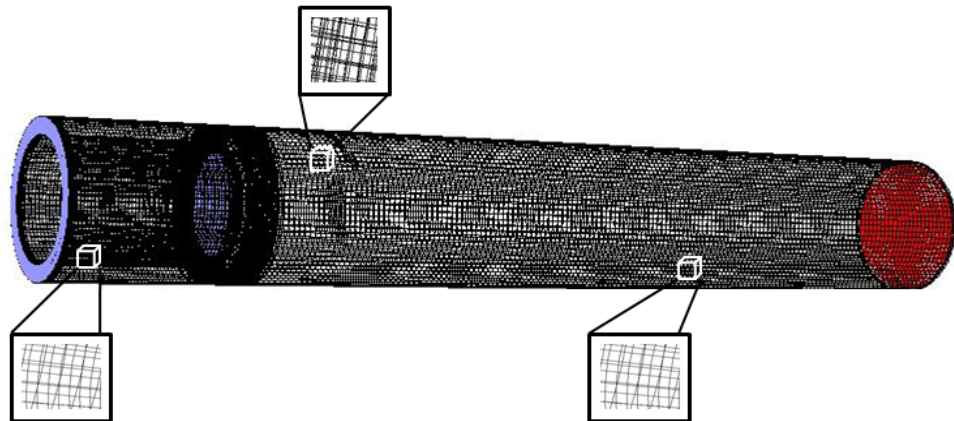
Figure4.3 Grid generation of the model for two-dimension

Figure4.4 Grid generation of the model for three-dimension

In this study, the resolution of 2-D structured grids was varied from coarse grid

(number of grids = 10089), medium grid (number of grids = 24,489), fine grid (number

of grids = 41,000), and to very fine grid (number of grids = 85,675). The information of

grid quality and grid quantity is shown in Table 4.1.
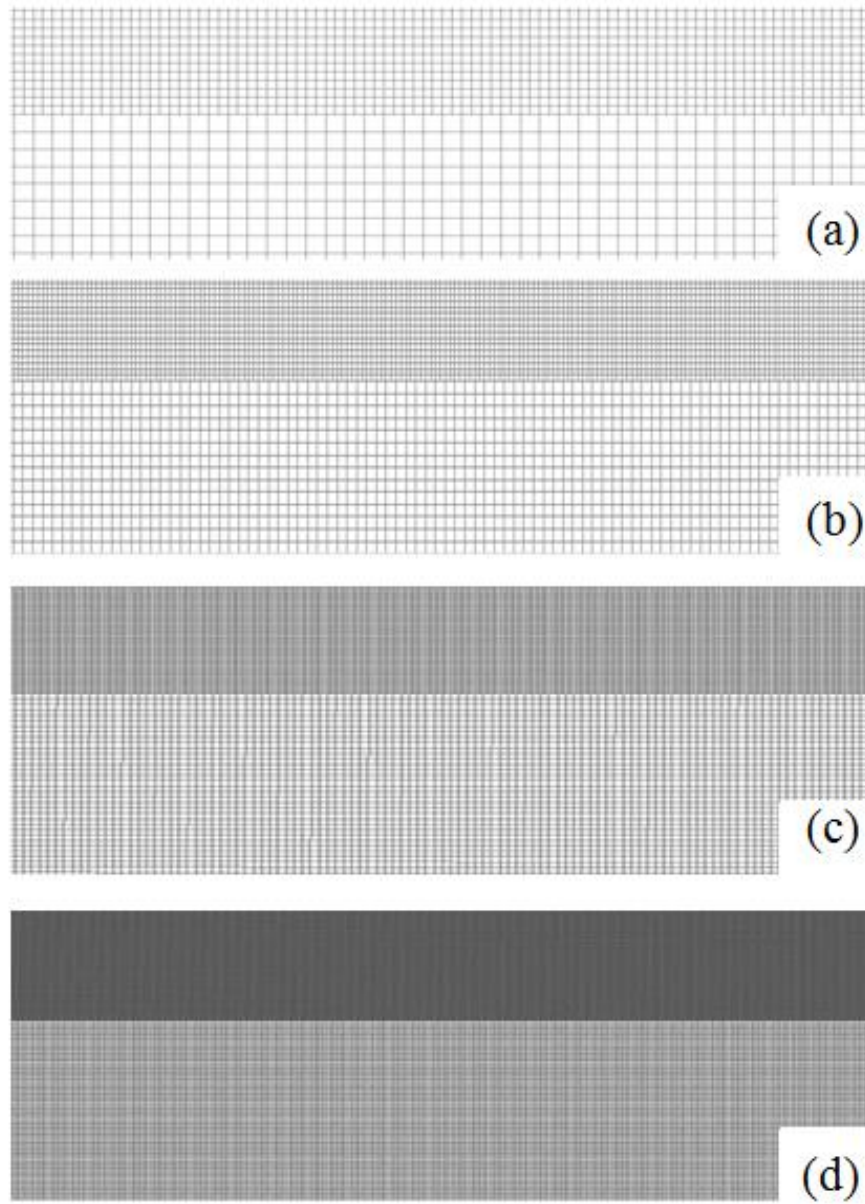
Figure4.5 Grid generation of the 2D model with grid number varied from:(a) 10089,

(b) 24489, (c) 41,000, and (d) 85,675

Table4.1 Grid quality and grid quantity for different grid number for 2D model

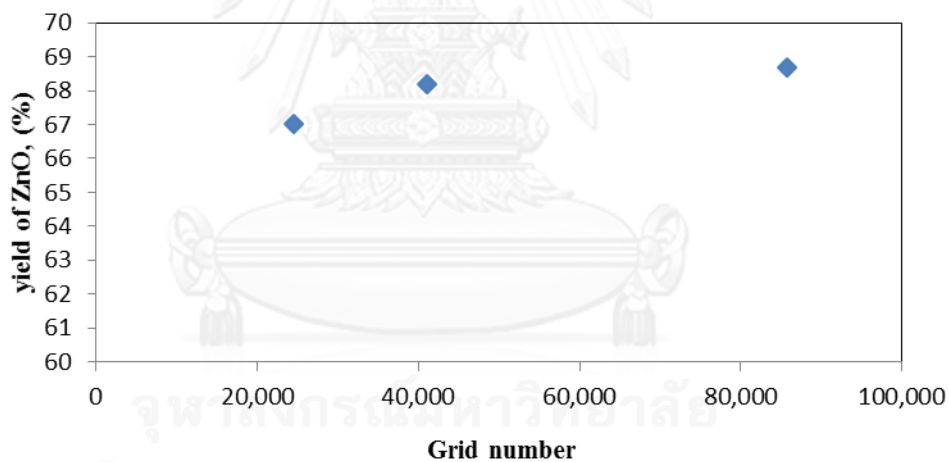| Cells	Operating time (hour)	Grid quality	
		Minimum Orthogonal	Maximum Aspect Ratio
10,089	0.3	8.94×10^{-1}	10
24,489	0.5	8.94×10^{-1}	12
41,000	1.5	8.94×10^{-1}	17
85,675	3	8.94×10^{-1}	30

Figure4.6 2-D model for calculated ZnO yields as a function

of number of grids.

For 2D model ,Fig 4.6 shows the deviation of the ZnO yields due to the variation of the grid resolution. The highest deviation of the predicted ZnO yields was found when the grid resolution was 10,089 (i.e., coarse grid). When the grid resolution was within the range of 24,489-85,675, the predicted ZnO yields was slightly changed

and became nearly constant. The difference between the predicted values of ZnO yields at the grid resolution of 24,489 and 85,675 was 14.1% and that at the resolution of 2,4489and 85,675 was 2.1%. As a result, the grid resolution of 24,489 was applied in this study.

In this study, the resolution of 3-D structured grids was varied from coarse grid (number of grids = 87,000), medium grid (number of grids = 270,000), fine grid (number of grids = 696,000), and to very fine grid (number of grids = 823,000). The information of grid quality and grid quantity is shown in Table 4.2.
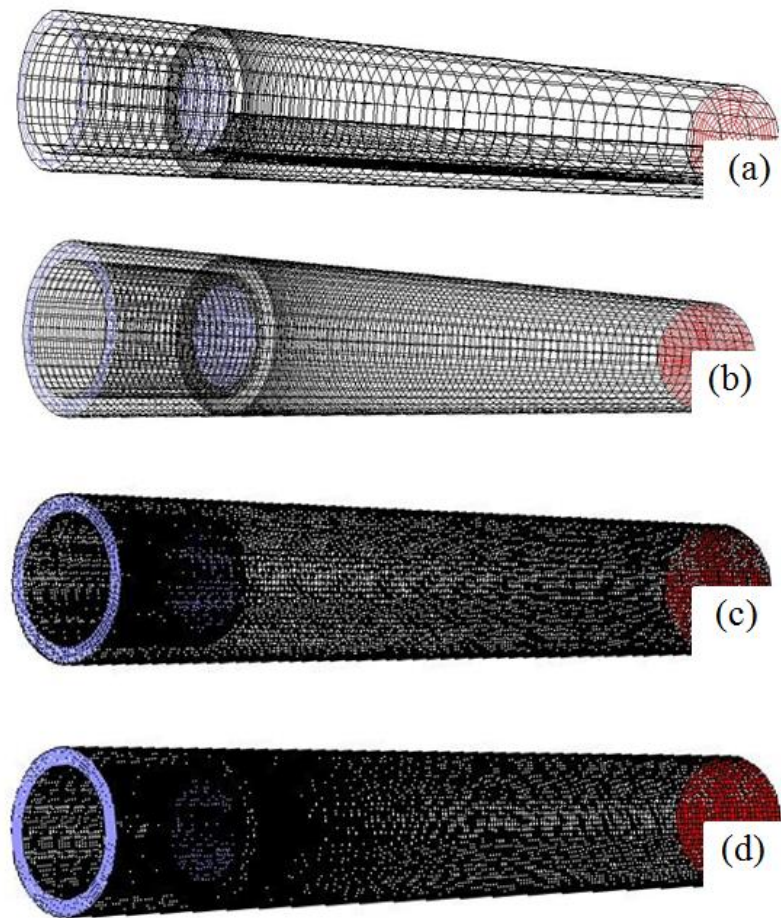
Figure4.7 Grid generation of the 3D model with grid number varied from: 87,000,

(b) 270,000, (c) 696,000, and (d) 823,000

Table4.2 Grid quality and grid quantity for different grid size for 3D model

Cells	Operating time (hour)	Grid quality	
		Minimum Orthogonal	Maximum Aspect Ratio
87,000	1.3	7.69×10^{-1}	11
270,000	4.2	7.60×10^{-1}	20
696,000	7.5	7.41×10^{-1}	30
823,000	13	7.69×10^{-1}	55
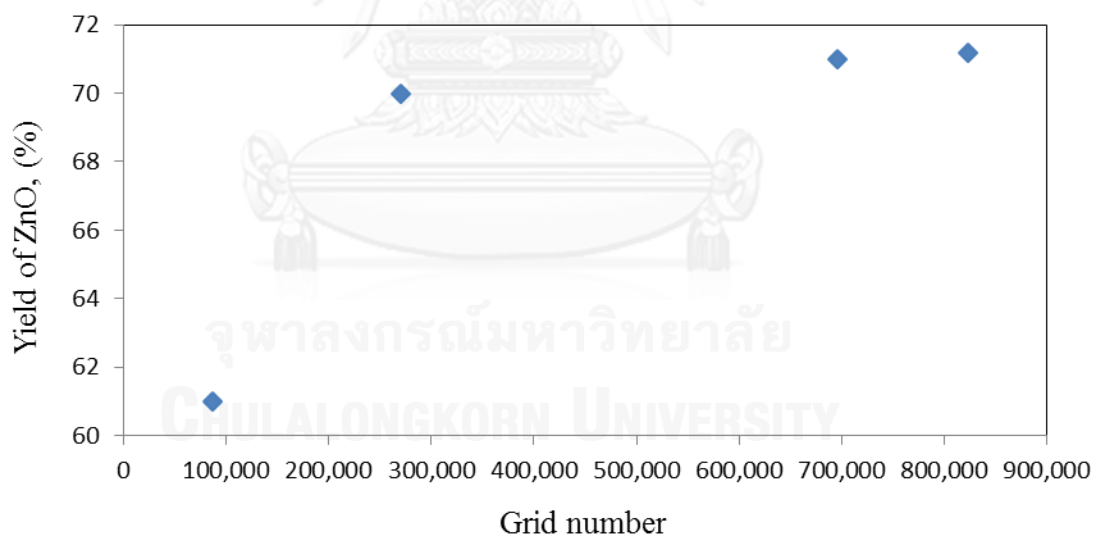
Figure4.8 3-D model for calculated ZnO yields as a function of number of grids

For 3D model, Figure 4.8 shows the deviation of the ZnO yields due to the variation of the grid resolution. The highest deviation of the predicted ZnO yields was

found when the grid resolution was 87,000 (i.e., coarse grid). When the grid resolution was within the range of 87,000 - 823,000, the predicted ZnO yields was slightly changed and became nearly constant. The difference between the predicted values of ZnO yields at the grid resolution of 87,000 and 823,000 was 14.3% and that at the resolution of 270,000 and 823,000was 1.68%. As a result, the grid resolution of 270,000 was applied in this study

The grid resolution have a great effect on the results of numerical simulation in a certain range. When considering grid-independent, a very dense grid can avoid this problem but the calculational resource may be wasted unnecessarily. From the results shown in Fig 4.6, Fig 4.8 and Table 4.1, Table 4.2, as the grid is increased ,the results more become accurate. Choose minimum grid for error acceptable that the numerical results change slightly and become nearly constant. Grid independent can save computational resource and time operating while ensuring a rational computational result. The truncation error caused by grid resolution is defined as the difference between the grid independent result $\Phi_{independent}$ and current numerical result Φ :

$$\varepsilon = \Phi_{independent} - \Phi \qquad (11)$$

According to previous studies, truncation error will become smaller and smaller by refining computational grid [25]

4.2 Validation of the model

CFD technique based on a three-dimensional (3-D) and axisymmetric two-dimensional (2-D) domain, non-isothermal model was employed for simulating ZnO synthesis using modified French method in a tubular reactor. The species mass transport equations with laminar finite reaction rate were employed to calculate yields of ZnO. The simulated results were validated by comparing with the experimental results. The boundary conditions (i.e., mass flow rate, temperature and mass fraction) in all simulations were setup corresponding to those in the experiments. The result of ZnO yield is presented in Figure 4.9 and the temperature profile is shown in Figure 4.10

The CFD model has been already validated in terms of yield of ZnO, for different operating conditions. Validation is an indication that the model predictions are valid and achieve
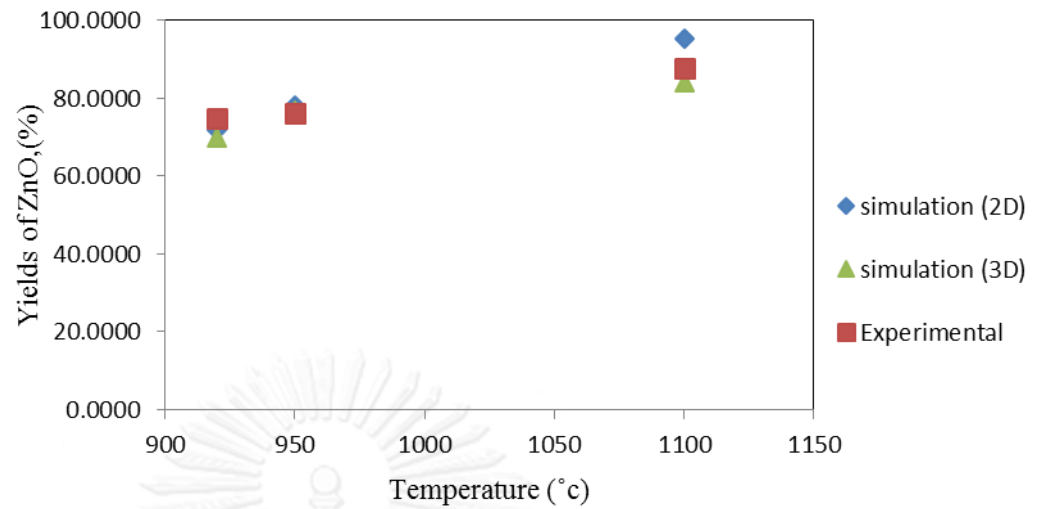
Figure4.9 Comparison between 2D and 3D simulated yields of zinc oxide and experimental data for different temperature
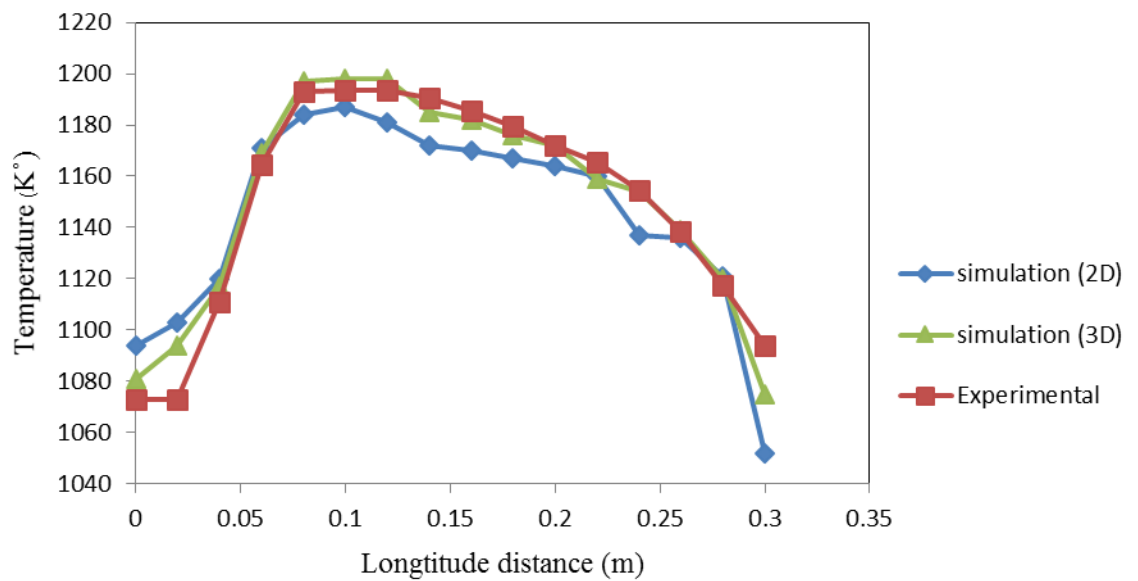

Figure4.10 Comparison between simulated temperature profile and experimental data for 2D and 3D

The simulation results were obtained for three different temperature. Figure 4.9 illustrates the comparison between the computed yields of zinc oxide for 2-D, 3-D and the experimental data for different temperature including 920 °C, 950 °C, and 1100 °C.

To validate the CFD model, yield of ZnO was simulated in the lab-scale tubular reactor using the experimental operating conditions. The yields of ZnO was obtained from the simulations by integrating the interesting domain compare with the experimental product data. The predicted results show good quantitative agreement with the experimental data for the yield of ZnO. The yield is over- predicted in the case of 2-D simulation and more similar to the experimental results in the case of 3-D simulation as shown in Figure 4.9.

Figure 4.10 shown comparison between simulated temperature profile and experimental data for 2D simulation and 3D simulation. The validation of CFD calculation results for temperature along the tubular reactor with experimentally measured values of temperatures profile using thermometer with the. From Fig. 4.10, it is observed that the value of temperature measured by thermometer is higher than CFD calculation results for both the 2D simulation and 3D simulation cases. The experimental measurement of temperatures good agreement with the CFD calculation results. The experimental measurement agreed reasonably well with the CFD predictions having deviation less than 5%.

Figure 4.11 - Figure 4.13 shown 2D model contours of temperature, mass fraction of zinc oxide and reaction rate for difference temperature at 920 °C, 950 °C, and 1100 °C. Figure 4.14- Figure 4.16 shows 3D model contours of temperature, mass fraction of zinc oxide and reaction rate on the two cross-sectional planes for difference temperature at 920 °C, 950 °C, and 1100 °C
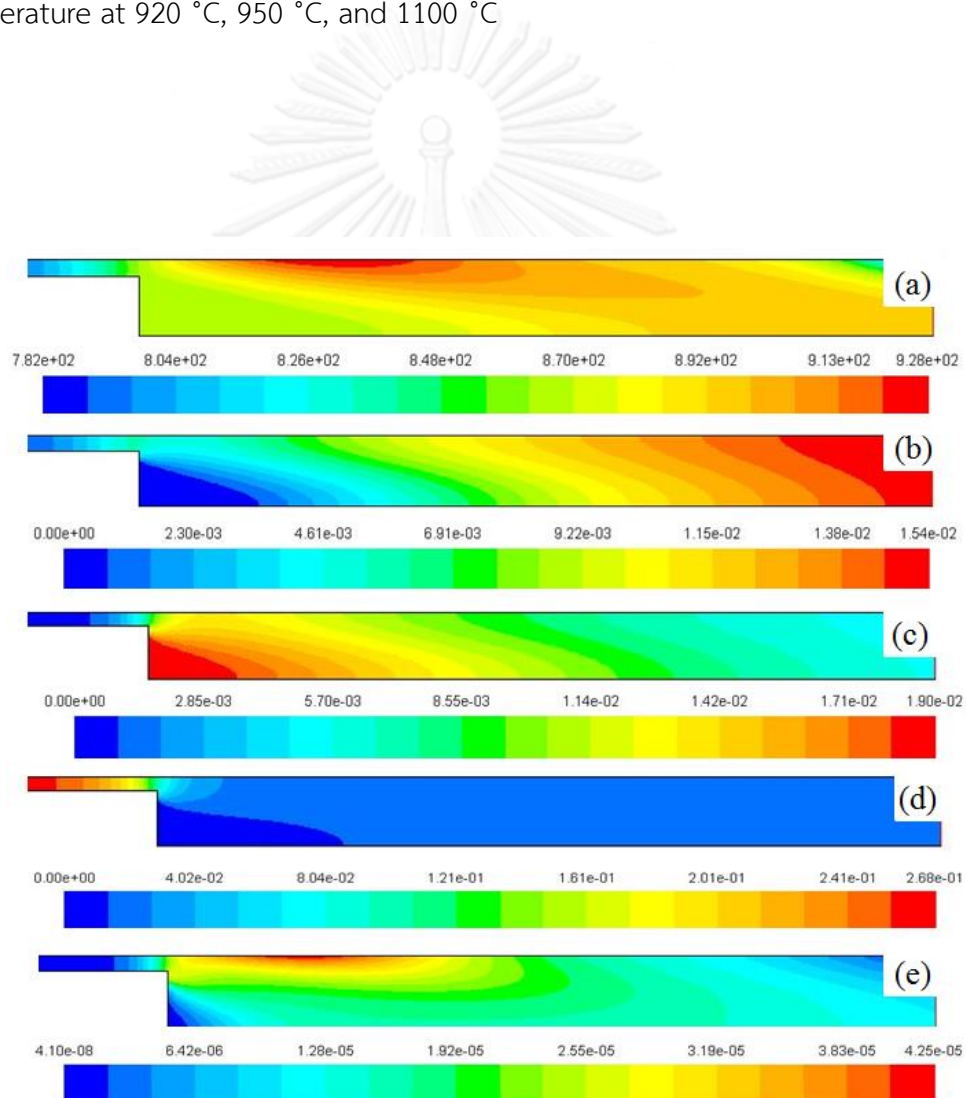

Figure4.11 The contours of (a) temperature(K) , (b) mass fraction of zinc oxide

(c) mass fraction of zinc , (d) mass fraction of oxygen and

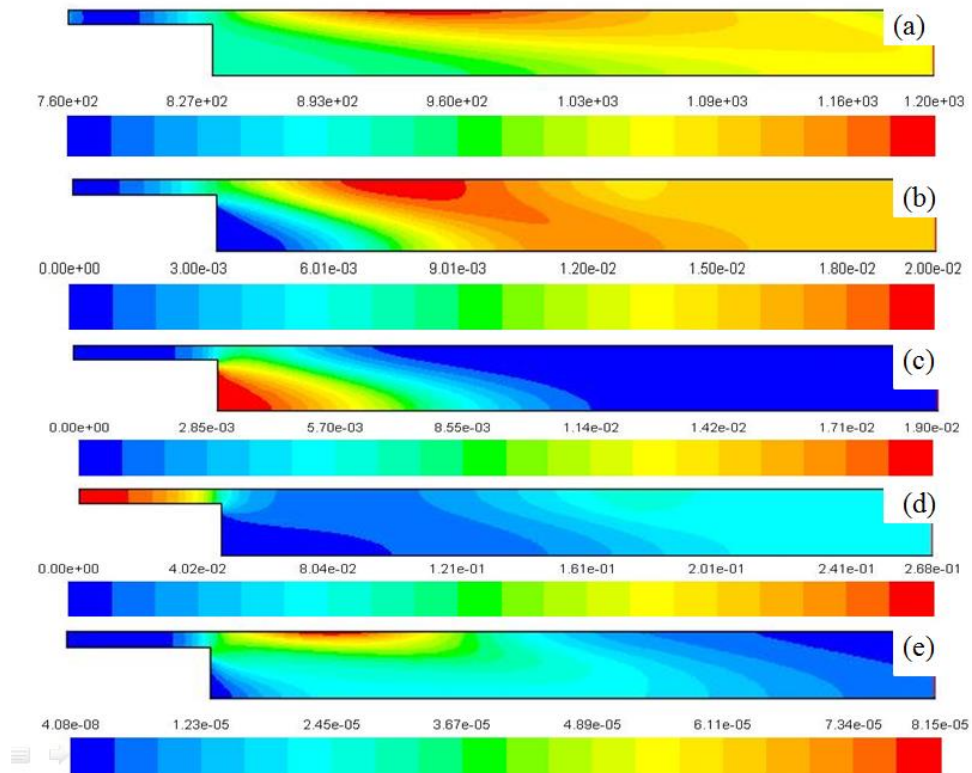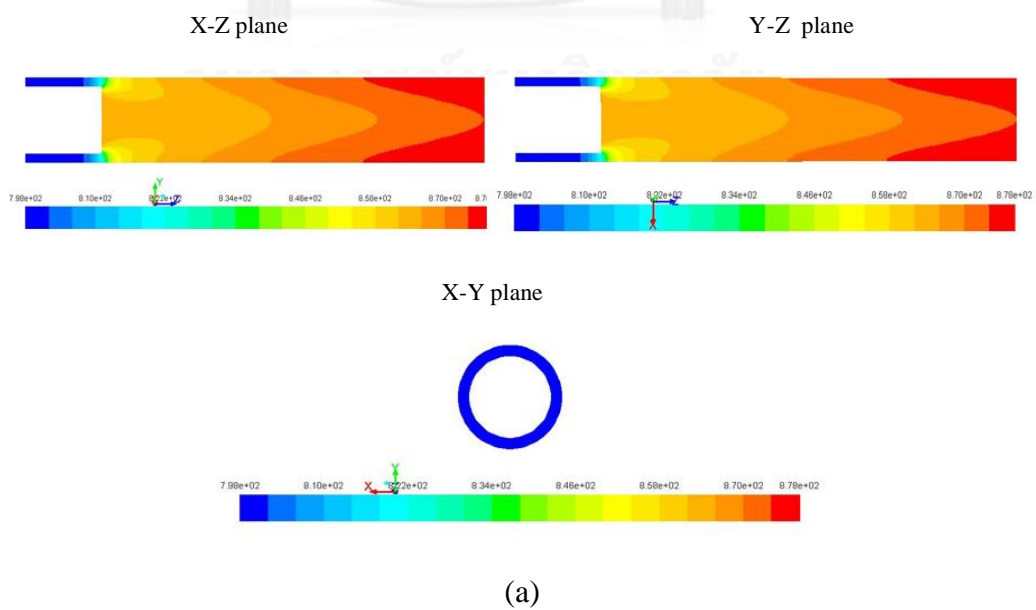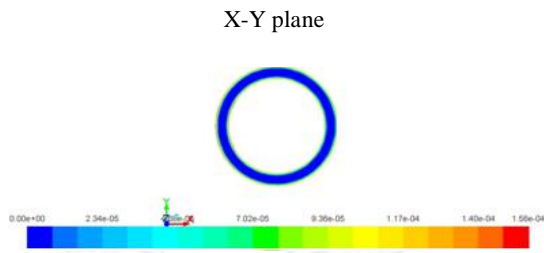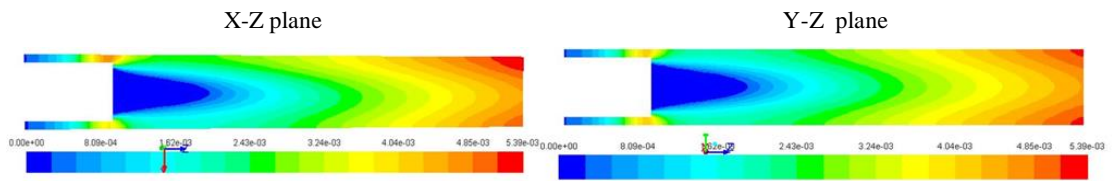(e) reaction rate (kmol/m^3. s) for temperature at 1,193 K
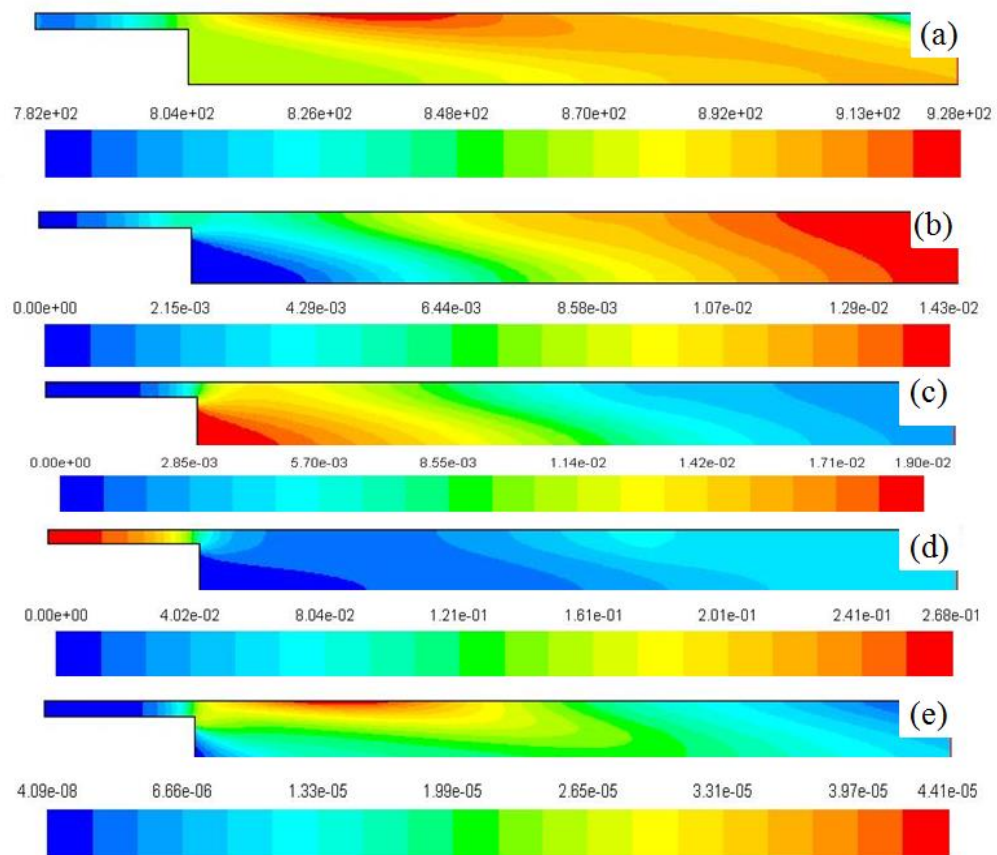
Figure4.12 The contours of (a) temperature (K), (b) mass fraction of zinc oxide,

(c) mass fraction of zinc , (d) mass fraction of oxygen and

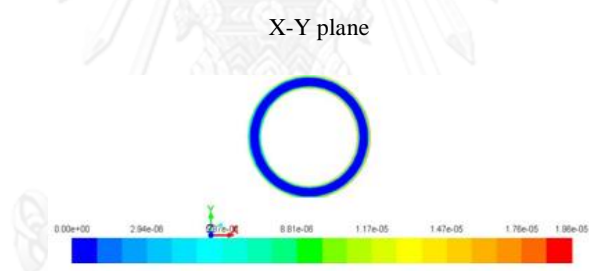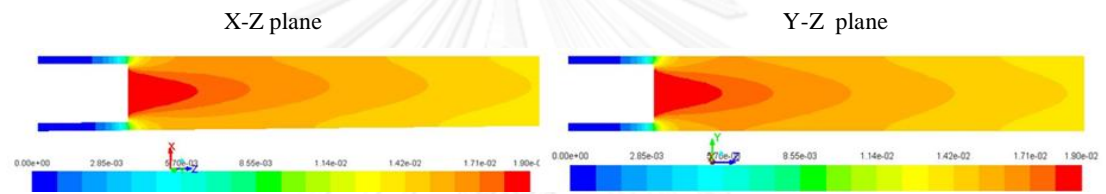(e) reaction rate (kmol/$m^3.s$) for temperature at 1,223 K

Figure4.13 The contours of (a) temperature (K), (b) mass fraction of zinc oxide

(c) mass fraction of zinc , (d) mass fraction of oxygen and

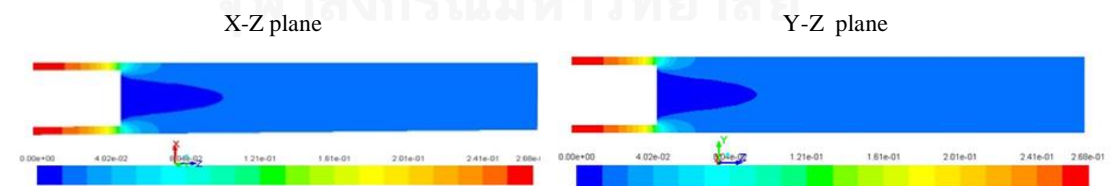(e) reaction rate(kmol/m^3.s) for temperature at 1,373 K

X-Z plane   Y-Z plane
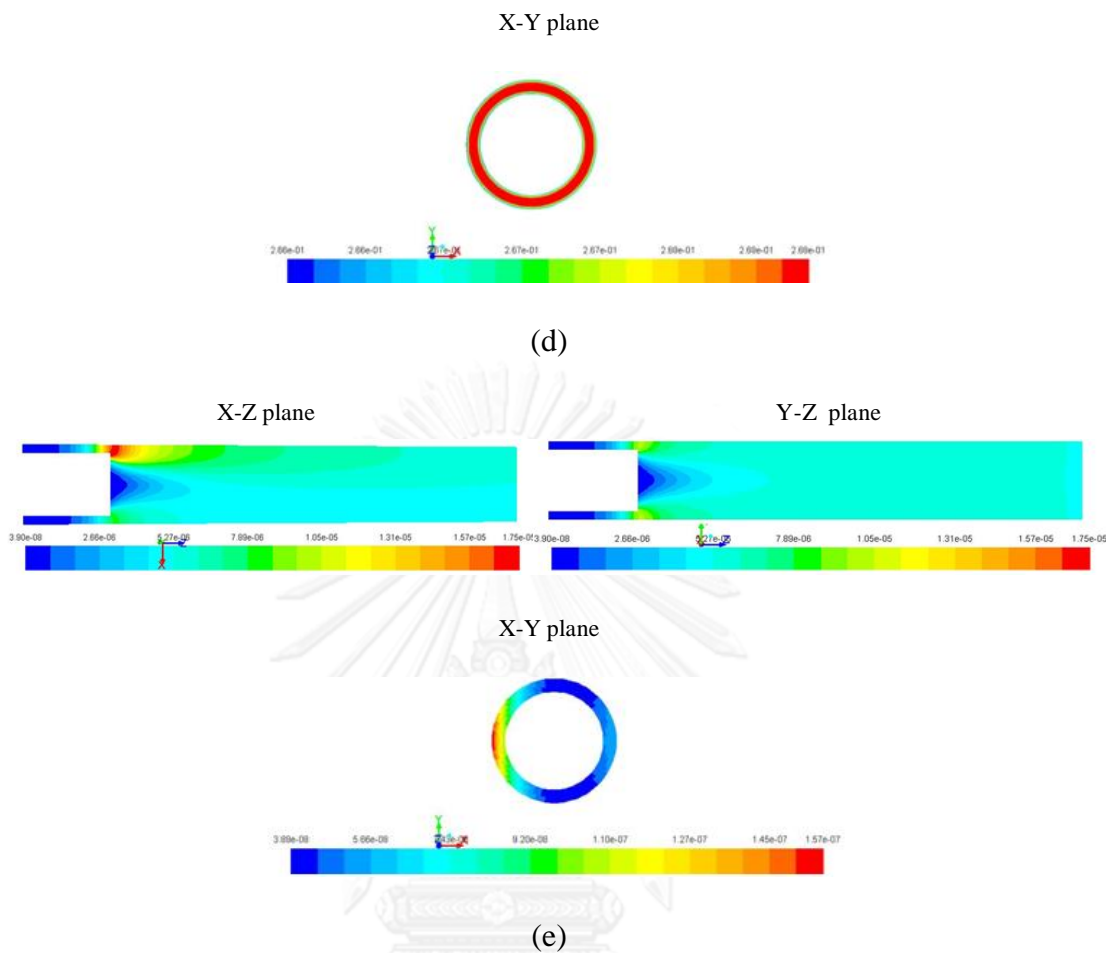

X-Y plane

(a)

X-Z plane   Y-Z plane

X-Y plane

(b)

X-Z plane   Y-Z plane

X-Y plane

(c)

X-Z plane   Y-Z plane

X-Y plane

(d)

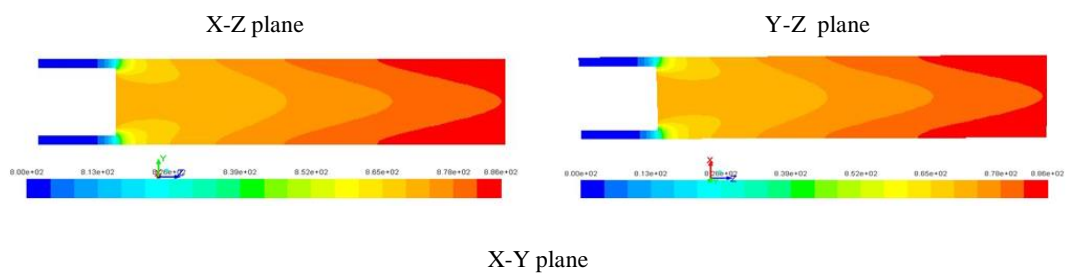X-Z plane   Y-Z plane

X-Y plane

(e)

Figure4.14 The contours of (a) temperature(K) , (b) mass fraction of zinc oxide(c) mass fraction of zinc , (d) mass fraction of oxygen and

(e) reaction rate of 3D model (kmol/$m^3.s$) on the cross-sectional x-z, y-z, and x-y plane respectively, for temperature at 1,193 K

X-Z plane   Y-Z plane

X-Y plane

(a)

X-Z plane   Y-Z plane

X-Y plane

(b)

X-Z plane   Y-Z plane

X-Y plane

(c)

X-Z plane   Y-Z plane

X-Y plane

(d)

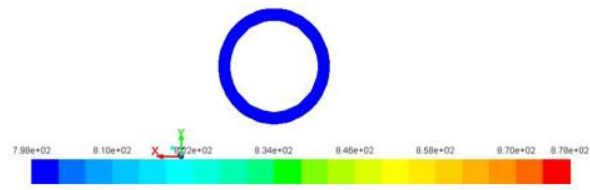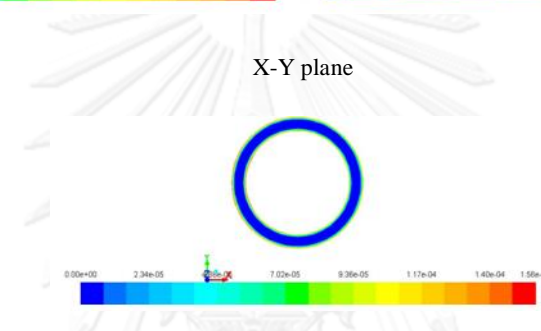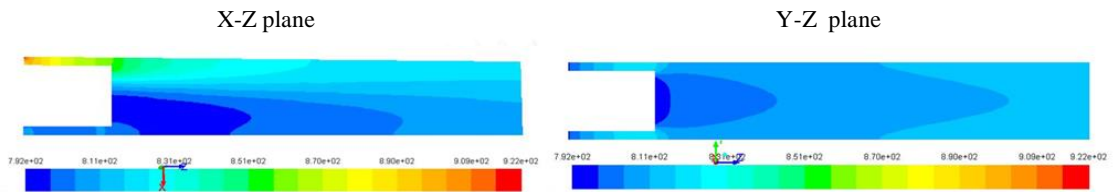X-Z plane   Y-Z plane

X-Y plane

(e)

Figure 4.15 The contours of (a) temperature (K) , (b) mass fraction of zinc oxide(c) mass fraction of zinc, (d) mass fraction of oxygen and

(e) reaction rate of 3D model (kmol/m^3.s) on the cross-sectional x-z, y-z, and x-y plane respectively, for temperature at 1,223 K
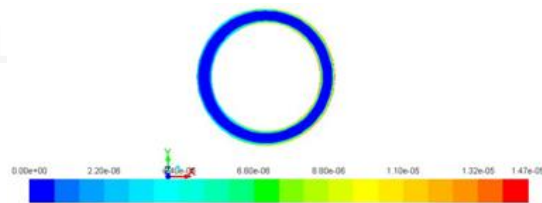
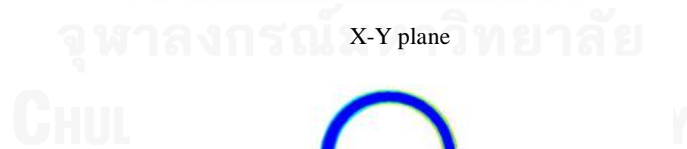X-Z plane   Y-Z plane

X-Y plane

(a)

X-Z plane   Y-Z plane

X-Y plane

(b)

X-Z plane   Y-Z plane

X-Y plane

(c)

X-Z plane   Y-Z plane

X-Y plane

(d)

X-Z plane   Y-Z plane

X-Y plane

(e)
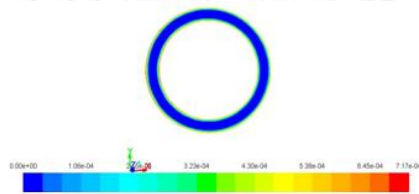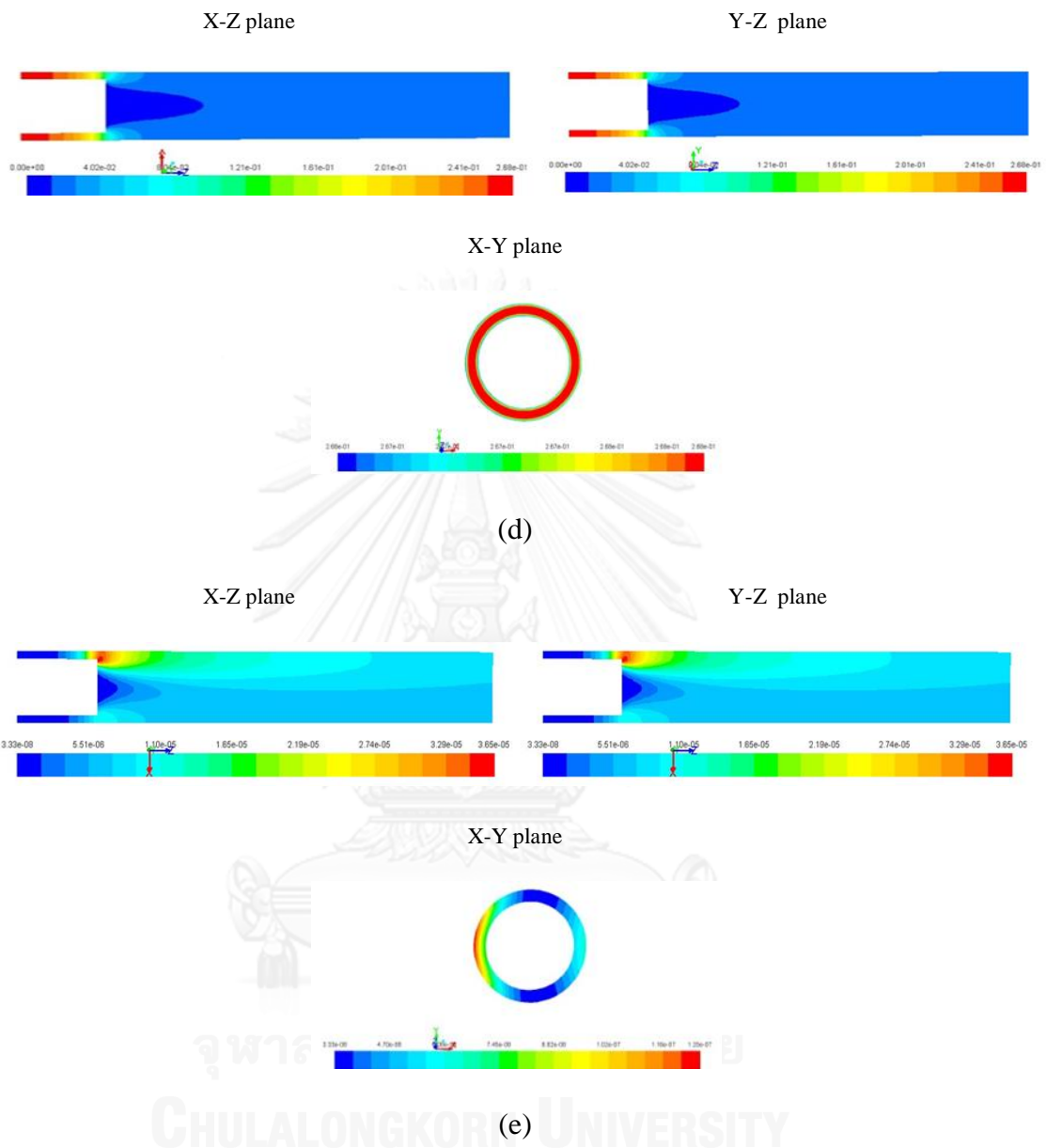
Figure4.16The contours of (a) temperature (K), (b) mass fraction of zinc oxide(c) mass fraction of zinc, (d) mass fraction of oxygen and

(e) reaction rate of 3D model (kmol/$\mathbf{m^3.s}$) on the cross-sectional x-z, y-z, and x-y plane respectively, for temperature at 1,373 K
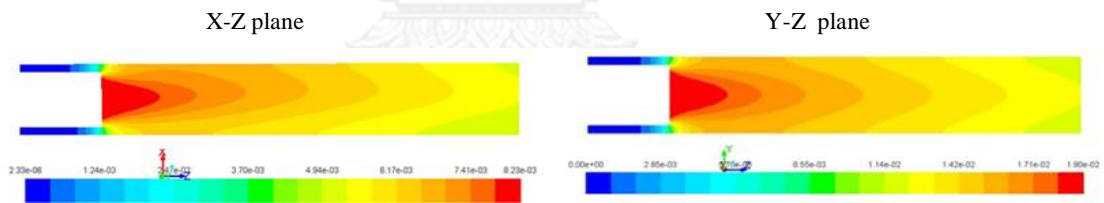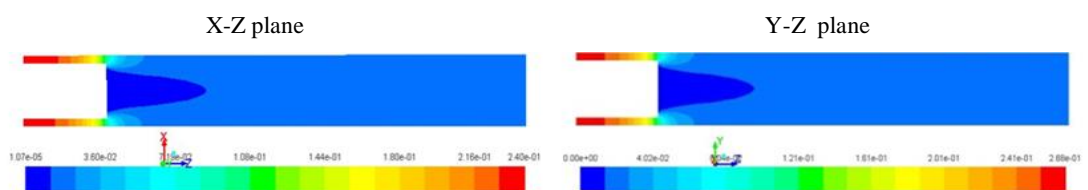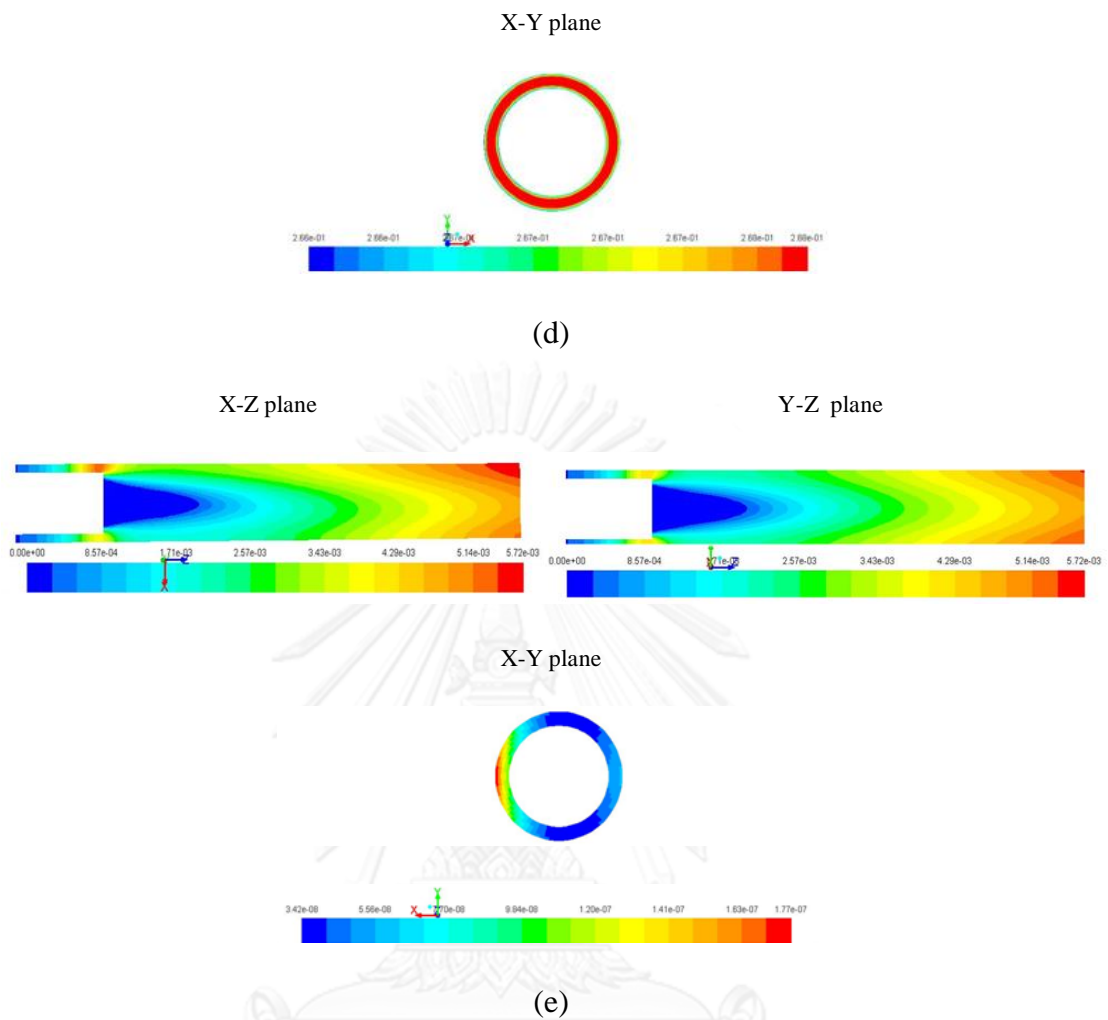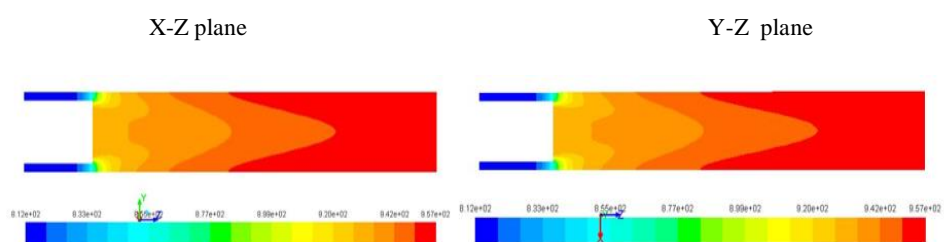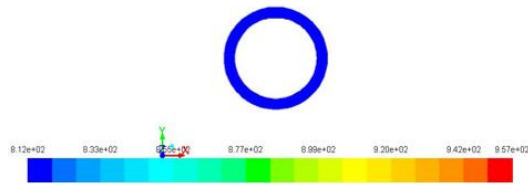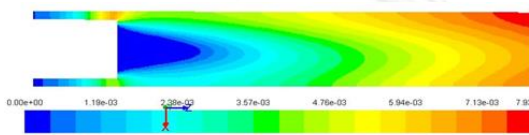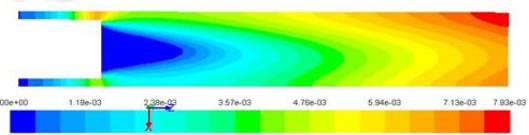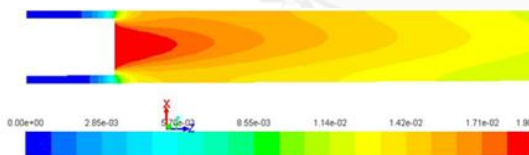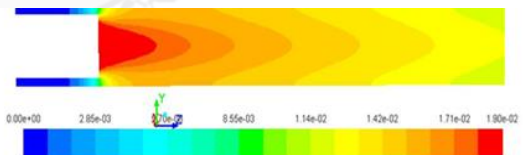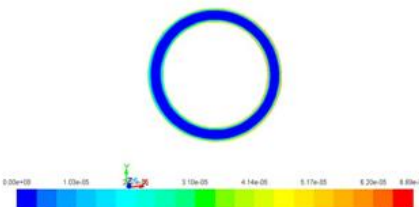
4.3.1. Description of temperature fields

Temperature distribution calculated by Fluent using volume integral method is presented in Figure 4.11(a) at 920 °C, Figure 4.11(b) at 950 °C, and 4.11(c) at 1,100 °C. It observed from temperature profile in the reactor, a hot spot located near the downsteam region of the reactor, because oxidation reaction is highly exothermic.

4.3.2. Description of mass fraction of zinc oxide fields

To predict the mass of ZnO, Figure 4.11(b) - Figure 4.16(b) compares the concentration distributions of ZnO at different temperatures. At the beginning of the reaction, mass fraction of ZnO occurred in the middle region because of Zn and O_2 mixing. Then with increasing Zn and O_2 mixing ,the mass fraction of ZnO was increased, caused by intensive mixing, and thus the efficiency of mass fraction is higher than in other regions, meaning that more Zn will be degraded. From the results that the high temperature enhances faster reaction between Zn vapor and oxygen so that ZnO more presence at the downstream zone.

4.3.3. Description of mass fraction of zinc and oxygen fields

Fig4.11(c) - 4.16(c) and Figure 4.11(d) - 4.16(d) display the mass fraction profile of reactant O_2 vapor and Zn vapor, respectively, as a function of position along the tubular reactor. Zn vapor and O_2 concentration gradually decrease further down the entrance in the reactor due to the rapid reaction between Zn vapor and oxygen.

However, large fraction of Zn vapor remains in the downstream and fraction of O_2 vapor is almost consumed after the entrance

4.3.4. Description of reaction rate fields

Fig 4.11(e) - Figure 4.16(e) show the reaction rates. From the picture shows completely alters the distribution of reaction rate especially near the wall that two stream first contact. The region with a high reaction rate is confined in the vicinity of flow O2/N2 mixture entrance. However, the region of reaction is extended to downstream.

Fig. 4.14, 4.15, and 4.16 show 3-D simulation results of temperature, mass fraction of zinc oxide, mass fraction of zinc, mass fraction of oxygen and reaction rate predicted by the ZnO synthesis model. The contours are comparable with a no significant differece between the 2D and 3D cases.

The error between the predicted yields of zinc oxide and the experimental data was less than 11% as shown in Table 4.3. Based on the results in Figure 4.9, and Table4.3, the computed yields of zinc oxide were in good agreement with the experimental data. The 3-D calculations showed better agreement with the experiments than the 2D axis-symmetric calculations, but they still underestimated the yield of ZnO because many assumptions was used in this model, resulting to some error occured.

.

Table4.3 Summary of the experimental and simulation results for

Different temperture

Temperature (°C)	Experimental yield (%)	2D Simulated yield (%)	% error	3D Simulated yield (%)	% error
920	74.74	67.00	10.36	71.2	4.74
950	76.15	78.00	2.43	77.56	1.85
1,100	87.60	95.27	8.76	91.43	2.08

4.3 Simulation of synthesis parameters which affect the yield of zinc oxide

4.3.1 Experimental results

For checking repeatability, two experiments were conducted under the same condition. In the 1st trial, the results obtained from previous experimental, However, in the 2nd trail, the experimental set-up was set for repeat and further investigate other condition, leading to an expectable result of high yield of white deposit along the quartz tube reactor. It could be clearly observed that all synthesized products collected exhibit purely white appearance. Similar to the results, microscopic analysis using XRD analysis would be further conducted to confirm its composition and purity of ZnO.

The yields of ZnO were dependent on the synthesis parameters such as reaction temperature and the nitrogen flow rate. The experiment was carried out to gathered ZnO at various conditions as shown in Table 4.4

Table4.4 Yield of ZnO at various conditions

Run	O_2 ml/min	N_2 ml/min	T evaporation (°C)	T oxidation (°C)	Yield (%)
1	32.5	0.1	800	920	74.74
2	32.5	0.1	800	950	76.14
3	32.5	0.1	800	1100	87.59
5	32.5	0.5	800	920	60.21
6	32.5	1	800	920	47.40
7	32.5	2	800	920	27.17

4.3.2 Effect of nitrogen flow rate

       With the confidence given by the model validation, the model was then employed to study the influence of different operating conditions on product yields, including nitrogen flow rate. For the effect of N_2 flow rate out of the range employed in previous experiments, the nitrogen flow rate has been varied between 0.05 lit/min to 4 lit/min, From Fig. 4.17, it was observed that the yield of ZnO increases with a decrease in N_2 flow rate. ZnO yield decrease when the nitrogen flow rate was higher, the residence time of the gas mixture in the reactor is relatively short, resulting in a decrease of the conversion rate. Moreover N2 flow is supplied to dilute the oxygen concentration, which is attributed to the incomplete oxidation and increase the partial pressure of O_2, resulting in a faster reaction between zinc vapor and O_2.
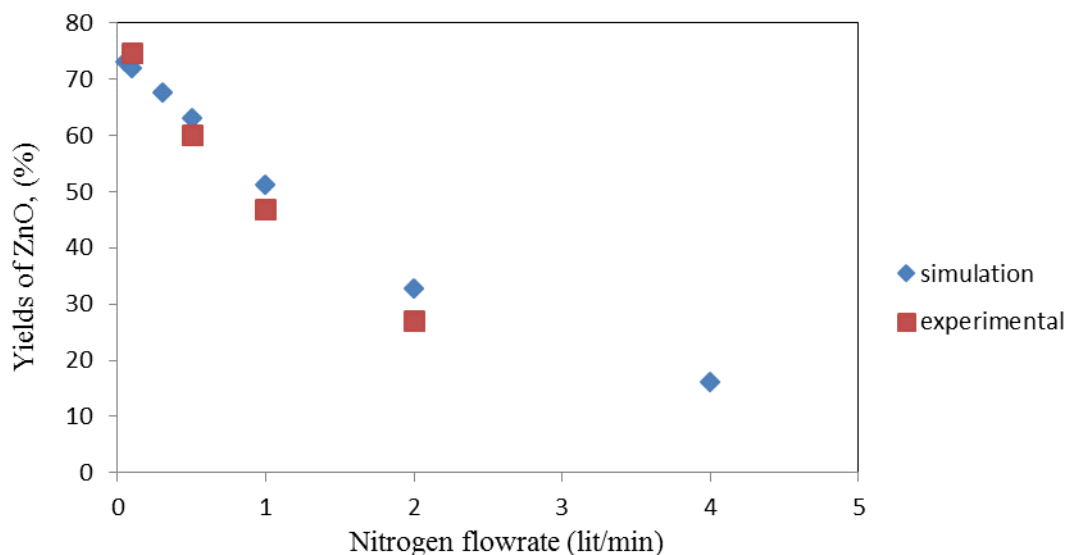

Figure4.17 Simulated results yield of ZnO at different N_2 flow rate

4.3.3 Effect of temperature.

The effect of temperature on ZnO yields obtained by varying the temperature between 650°C and 1200°C. The effects of temperature on yields of ZnO are given in Fig 4.18. From Fig.4.18, it can be seen that the ZnO yields increased with increasing the temperature. The simulated results revealed that the temperature strongly affected ZnO yields at the temperature between 650 °C to 1,100 °C and slightly affected ZnO yields at the temperature higher than 1,100 °C. In other words, the ZnO yields were found to significantly increase at low temperature range (600-1,100 °C). After the first region, the ZnO yields were slightly increased and found to be constant. Because the reaction rate increases with increasing the temperature. However, an increasing in the temperature was not necessary to improve the ZnO yields at high temperature level because amount of energy obtainable through this system is limited. From the results, it is clear that the temperature is an important design parameter for ZnO synthesis
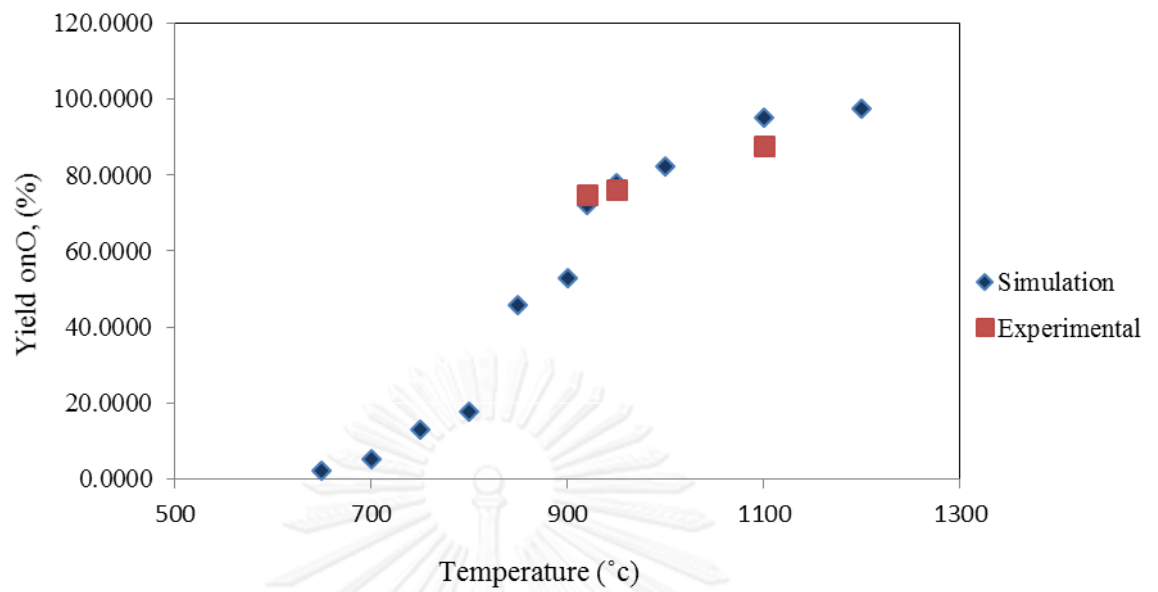
Figure4. 18 Simulated results yield of zinc oxide at different temperature

CHAPTER V

CONCLUSION AND RECOMMENDATION

5.1 Conclusions

In this study, CFD technique was employed to investigate the performances of 2-D and 3-D numerical simulations for ZnO synthesis using gas-phase reaction within a tubular reactor. The 2-D versus 3-D simulations were validated with respect to yield of ZnO. The results of simulation revealed that a 3-D simulation is suitable to predicted yield of ZnO when very accuracy are considered. And then further analysis was carried out to investigate the effect of N_2 flow rate and temperature on synthesizing yield of ZnO using non-isothermal model. The boundary conditions in all simulations were setup corresponding to the experiments. This model makes use of a series of the equation of continuity, momentum, energy and species mass balance. The simulation results were validated with experimental data reported in other previous works. A good agreement with the experimental data of ZnO yield indicates the validity of the model. The conclusions of the present research are summarized as follows:

- For the effect of N_2 flow rate out of the range employed in previous experiments, it was observed that the yield of ZnO increases with a decrease in N_2 flow rate. This result would be attributed to the dilution of N_2 which

would increase the partial pressure of O_2, resulting in a faster reaction between zinc vapor and O_2.

- For the effect of temperature on ZnO yeilds, the increasing in temperature leads to increase the yield of ZnO nanoparticles because the higher temperature delivers more energy into the system and increases the reaction rate. However, the increasing in ZnO yields was limited at the high temperature level.

5.2 Recommendation for Future Work

1 This study gives better understanding of the flows within the tubular reactor with porous tube. However flow domain for this study do not cover overall region of tubular reactor. There are still have flow domain for improvement the model to be more realistic.

2 Use unsteady state instead of steady state to eliminate the error resulting from steady state

REFERENCES

[1]   Versteeg, H. K., and Malalasekera, W. <u>An introduction to computational</u> <u>fluid dynamics The finite volume method</u>. Malaysia: Prentice Hall, 1995.

[2]   Kaya, F., and Karagoz, I. Numerical investigation of performance   characteristics of a cyclone prolonged with a dipleg. <u>Chemical Engineering Journal</u> 151 (2009) : 39-45.

[3]   Wanthamanee, S., Bumrungthaichaichan, E., and Wattananusorn, S. Influence of Turbulence promoter Geometry on Flow Pattern in Cross-Flow Membrane Ultrafiltration.   <u>Ladkrabang   Engineering   Journal</u>   29   (2012): 48-53.

[4]   Reuge, N., Bacsa, R., Serp, P., and Caussat, B. Chemical Vapor Synthesis of Zinc Oxide Nanoparticles: Experimental and Preliminary Modeling Studies.   <u>Journal of Physical Chemistry C</u> 113 (2009): 19845-19852.

[5]   Nijemeisland, M., and Dixon, A. G. Comparison of CFD simulations to experiment for convective heat transfer in a gas–solid fixed bed. <u>Chemical Engineering Journal</u> 82 (2001): 231-246.

[6]   Urgessa, Z. N., Oluwafemi, O. S., and Botha, J. R. Effect of precursor concentration on the growth of zinc oxide nanorod arrays on pre-treated substrates. <u>Physica B</u> 407 (2012): 1543–1545.

[7]   Yu, W., and Pan, C. Low temperature thermal oxidation synthesis of ZnO nanoneedles and the growth mechanism. <u>Materials Chemistry and Physics</u> 115 (2009): 74–79.

[8]   Lim, Y. S., Park, J. W., Hong, S. T., and Kim, J. Carbothermal synthesis of ZnO nanocomb structure. <u>Materials Science and Engineering B</u> 129 (2006): 100–103.

[9]   Shen, L., Zhang, H., and Guo, S. Control on the morphologies of tetrapod ZnO nanocrystals. <u>Materials Chemistry and Physics</u> 114 (2009): 580–583.

[10] Rosina, M., Ferret, P., Jouneau, P. H., Robin, I. C., Levy, F., Feuillet, G., and Lafossas, M. Morphology and growth mechanism of aligned ZnO nanorods grown by catalyst-free MOCVD. <u>Microelectronics Journal</u> 40 (2009): 242–245.

[11] Zong, X., and Wang, P. Effect of UV irradiation on the properties of ZnO nanorod arrays prepared by hydrothermal method. <u>Physica E</u> 41 (2009): 757–761.

[12] Wang, S., Xia, G., Shao, J., and Fan, Z. Structure and UV emission of nanocrystal ZnO films by thermal oxidation of ZnS films. <u>Journal of Alloys and Compounds</u> 424 (2006) : 304–306.

[13] Kim, S., Jeong, M., Oh, B., Lee, W., and Myoung, J. Fabrication of Zn/ZnO nanocables through thermal oxidation of Zn nanowires grown by RF magnetron sputtering. <u>Journal of Crystal Growth</u> 290 (2006): 485–489.

[14] Charnhattakorn, B., Charinpanitkul, T., Sirisuk, A., and Pavarajarn, V. Controlled synthesis of defects-containing ZnO by the French process modified with pulsed injection and its luminescence properties. <u>Ceramics International</u> 37 (2011): 2021–2024.

[15] Yamamoto, H., Otani, Y., Seto, T., Nartpochananon, P., and Charinpanitkul, T. Generation of uniform tetrapod-shaped zincoxide nanoparticles by gas-phase reaction with using flow restrictor. <u>Advanced Powder Technology</u> 23 (2012): 71-79.

[16] OH, H. W. <u>Computational Fluid Dynamics</u>. India: InTech, 2010.

[17] Socolofsky, S. <u>Lecture note on Fluid Dynamics for Ocean and Environmental Engineering</u>. TEXAS A&M UNIVERSITY, 2012.

[18] Bird, R. B., Stewart, W. E., and Lightfoot, E. N. <u>Transport Phenomena</u>. 2nd edition. USA: Wiley, 2007.

[19] ANSYS, Inc. <u>ANSYS FLUENT 12.0 Theory Guide</u>. 2009.

[20] Wilkes, J. O. <u>Fluid Mechanics for Chemical Engineers, 2nd ed., with microfluidics and CFD</u>. 2nd edition. Massachusetts: Prentice Hall, 2006.

[21] Cushman-Roisin, B. <u>ENVIRONMENTAL FLUID MECHANICS</u>. USA: Wiley, 2010.

[22]Wang, X., and Tan, S. K. Environmental fluid dynamics-jet flow. 9th International Conference on Hydrodynamics (ICHD 2010), Shanghai, China, October 11-15, 2010.

[23]Gutmark, E. J., and Grinstein, F. F. FLOW CONTROL WITH NONCIRCULAR JETS[1]. Annual Review of Fluid Mechanics 31 (1999): 239–272.

[24]Seok, J. K., and Il, W. S. Reynolds number effects on the behavior of a non-buoyant round. Experiments in Fluids 38 (2005): 801-812.

[25]Yang, J., Sodabanlu, H., Waki, I., Sugiyama, M., Nakano, Y., and Shimogaki, Y. Process design of the pulse injection method for low-temperature metal organic vapor phase epitaxial growth of AlN at 800 °C. Journal of Crystal Growth 311 (2009): 383–388.

[26]Zhang, J., Yang, Y., Xu, B., Jiang, F., and Li, J. Shape-controlled synthesis of ZnO nano- and micro-structures. Journal of Crystal Growth 280 (2005: 509–515.

[27]Hsu, Y. F., Djurisic, A. B., and Tam, K. H. Morphology and optical properties of ZnO nanostructures grown under zinc and oxygen-rich conditions. Journal of Crystal Growth 304 (2007): 47–52.

[28]Welty, J. R., Wicks, C. E., Wilson, R. E., and Rorrer, G. L. Fundamentals of Momentum, Heat, and Mass Transfer. 5th edition. USA: Wiley, 2008.

[29]Kliem, S., Höhne, T., Rohde, U., and Weiss, F. P. Experiments on slug mixing under natural circulation conditions at the ROCOM test facility using high-resolution measurement techniques and numerical modeling, Nuclear Engineering and Design. 240 (2010): 2271–2280.

[30] Stern, F., Wilson, R. V., Coleman, H. W., and Paterson, E. G. VERIFICATION AND VALIDATION OF CFD SIMULATIONS. IIHR Report No. 407. Iowa: Iowa Institute of Hydraulic Research, 1999

APPENDIX

APPENDIX A

C-CODE OF TEMPERATURE PROFILE

```
#include "udf.h"

DEFINE_PROFILE (temp_wall,thread,position)

{

        realr[3];

        realx;

        face_t 1;

        begin_f_loop(1,thread)

            {

            F_CENTROID(r, 1, thread);

            x = r [0];

            F_PROFILE (1, thread, position) = 229049.89*x*x*x*x*x*x -

    401566.64*x*x*x*x*x + 255764.26*x*x*x*x                          -

70248.54*x*x*x + 2711.18*x*x + 2616.07*x + 650.54;
```
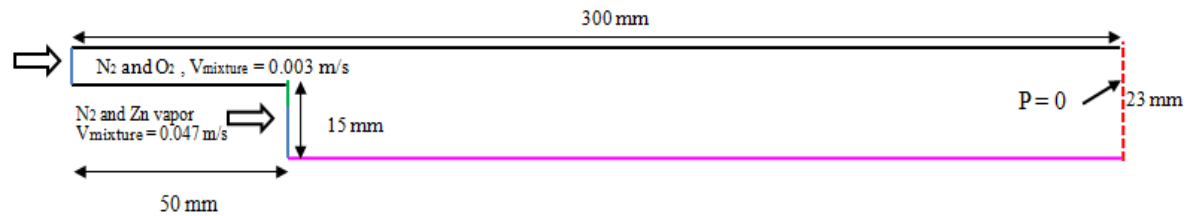
```
            }

    end_f_loop (1,thread)


}
```

APPENDIX B

GAMBIT

FigureB.**1** Domain and boundary conditions for 2D model
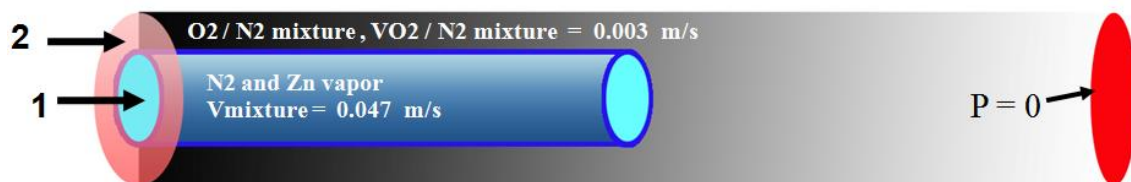
FigureB.**2** Domain and boundary conditions for 3D model

1 Specify boundary conditions for 2D model and 3D model

There are many boundary conditions in this model as shown in Figure B.1 and Figure B.2. The blue line, red line, green line, gray line and pink line are velocity inlet boundary type, pressure outlet type, interior type, and wall type, axis respectively.

1.1   Setting inlet boundaries (blue lines). Velocity inlet boundary type can be set

as shown in Figure B.1 and Figure B.2. The details of inlet boundary are shown

in Table B.1.
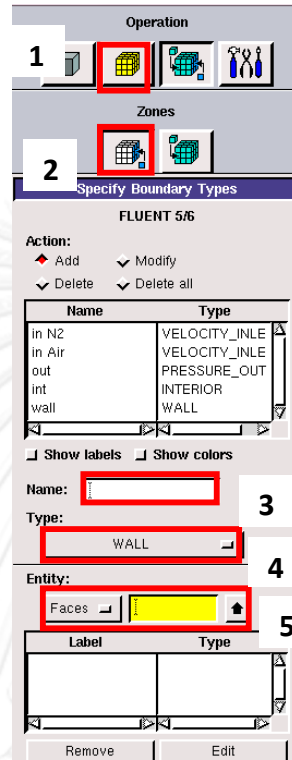
FigureB.3 Specify boundary conditions

TableB.1 Details of inlet boundaries

| Number	Name	Type
Stream 1	N2 + Zn vapor	VELOCITY_INLET
Stream 2	N2+O2 Flow	VELOCITY_INLET

1.2 Setting outlet boundary (red line) as PRESSURE_OUTLET

1.3. Setting interior boundary (green line) as INTERIOR
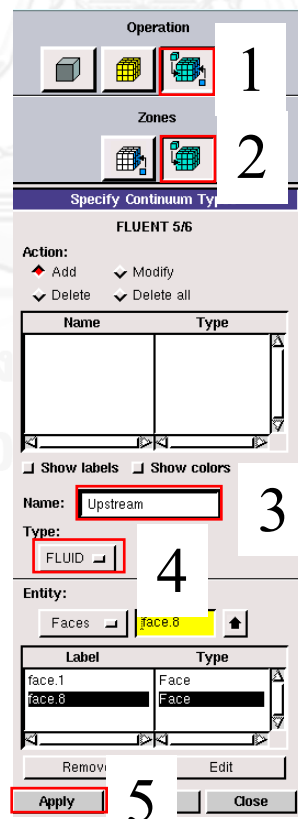
1.4. Setting wall boundary (black line) as WALL

1.5 Setting wall boundary (pink line) as AXIS for 2D model

2 Specify continuum zones

These model consists of two zones, including upstream and reaction zones as shown in Figure B.4. The continuum setting is shown in Figure B.5.
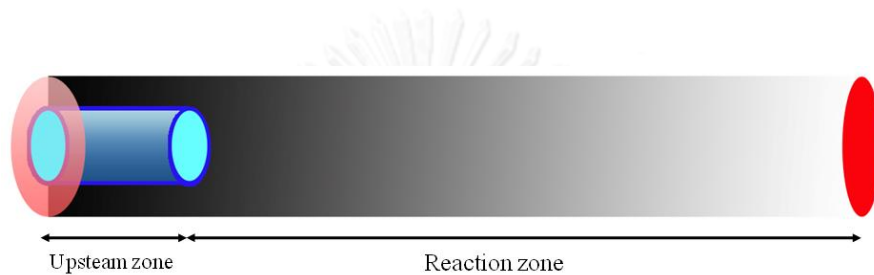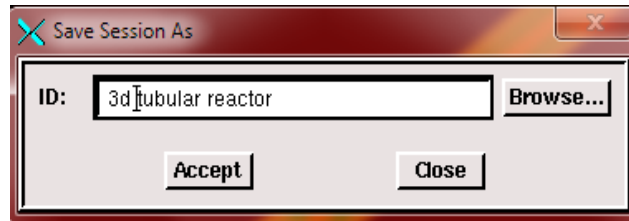

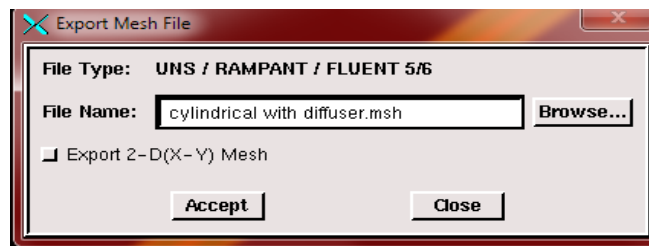FigureB.4 Zones of the model

FigureB.5 Specify continuum type

3 Save the model as shown in Figure B.6

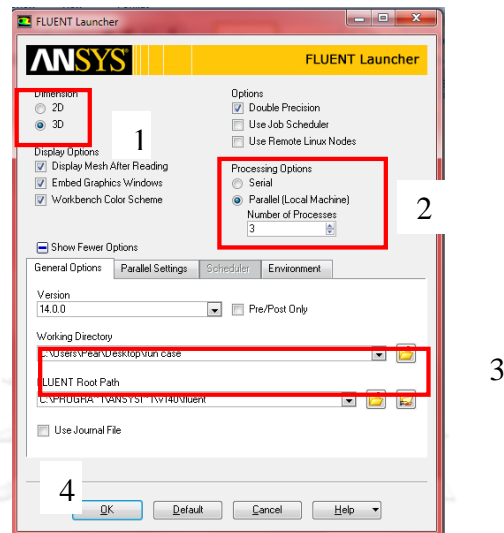4 Export the mesh as shown in Figure B.7
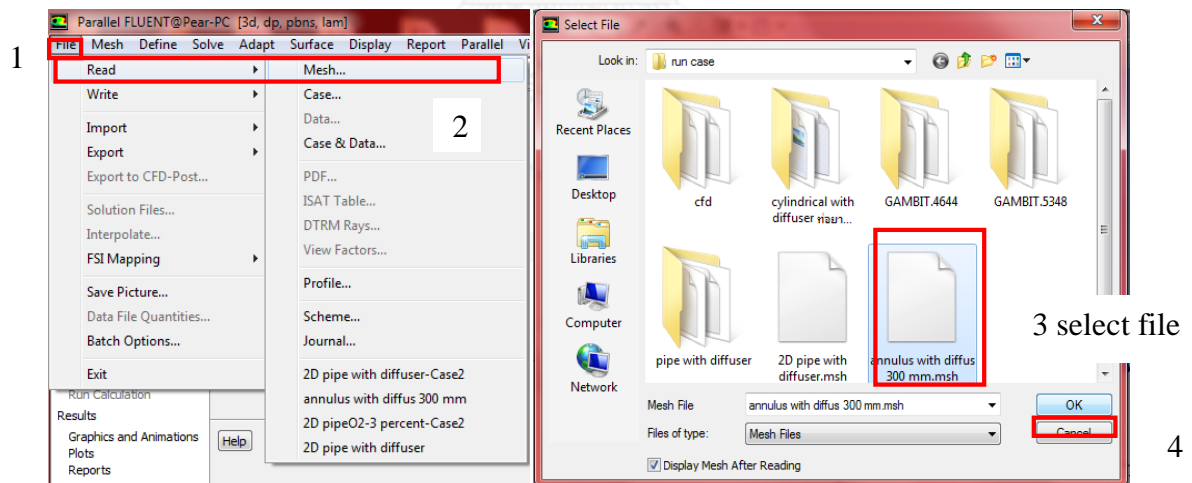

5   Finish and close GAMBIT

APPENDIX C

SIMULATION IN FLUENT

1 Open FLUENT and setting FLUENT Launcher as shown in Figure C.1.

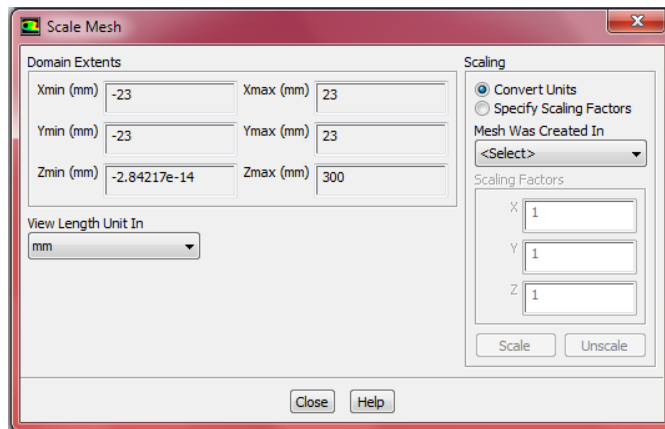FigureC.1 FLUENT Launcher setting

2 Read the existing mesh files as shown in Figure C.2.

FigureC.2 Select mesh file step

3. General setting

    3.1 Scale the model. Mesh > Scale > Mesh was created in > mm > Scale > Close

    3.2 Check mesh. Mesh > Check

    3.3 Solver setting. Select the solver as shown in Figure C.3
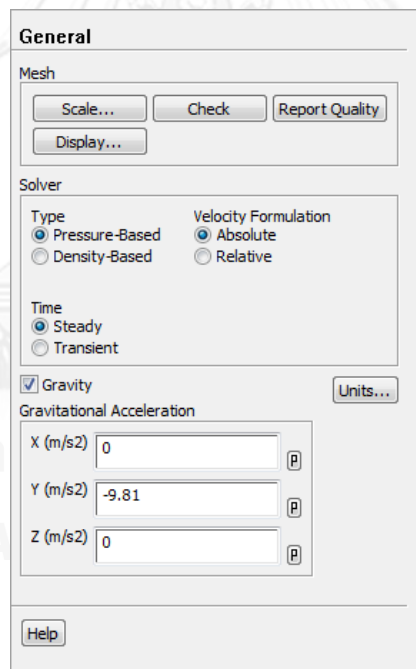

FigureC.3 Solver setting
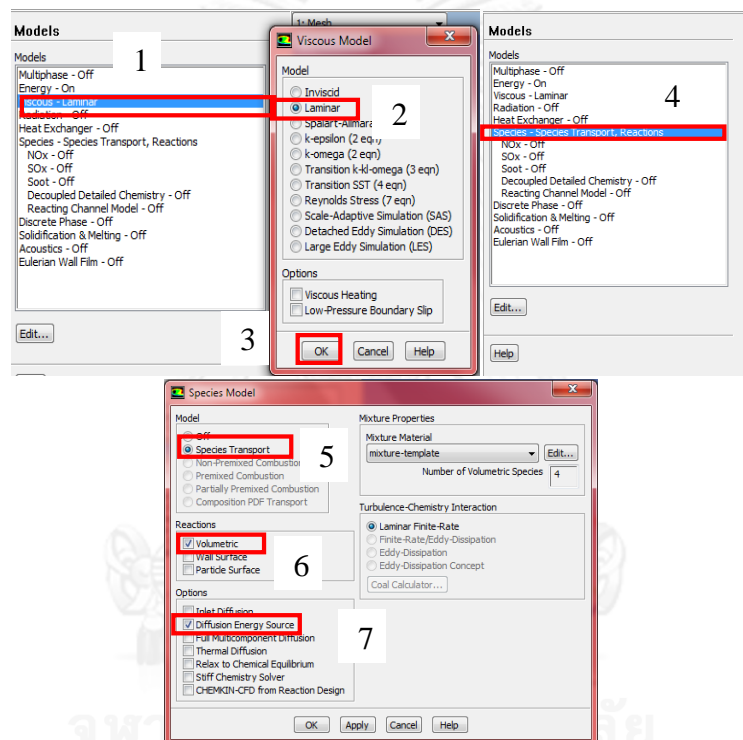
4 Models selection

    4.1 Turn on energy equation. Models > Energy > Edit >

       Select Energy equation >   OK

    4.2 Select larminar model Models > Viscous > Edit > laminar > OK

    4.3 Select species. Models > Species > Edit > Select species transport > Select

       volumetric for reactions > Select Laminar Finite-rate > OK

5 Material setting

    Create Zn vapor and ZnO in Fluid materials section. This step can be shown in

Figure C.4. The gases properties and gases properties setting are shown in Table C.1 and

Table C.2, respectively.

FigureC.4 Material creation

TableC.1 Gases properties

Properties	Unit	Coefficient	Gases			
			Nitrogen	Oxygen	Zinc	Zinc oxide
Formular			N_2	O_2	Zn	ZnO
Density @ 300K	[kg/m^3]		1.145	1.308	-	-
Molecular weight	[kg/kmol]		28.013	31.999	65.39	81.389
Standard state enthalpy	[J/kgmol]		0	0	1.304e8	0
Standard state entropy	[J/(kgmol-K)]		191494.8	205026.9	160980	43640
Specific heat		A	-	-	323.108	300.483
Cp=A+BT+CT2+DT3+ET4	[J/(kg-K)]	B	-	-	-2.034E-02	4.299E-01
		C	-	-	1.126E-05	-4.885E-04
		D	-	-	-2.723E-09	2.503E-07
		E	-	-	2.520E-13	-4.650E-11

TableC.2 Gases properties setting

Properties	Unit	Gases			
		Nitrogen	Oxygen	Zinc	Zinc oxide
Formular		N_2	O_2	Zn	ZnO
Heat capacity (Cp)	[J/(kg-K)]	Polynomial	Polynomial	Polynomial	Polynomial
Thermal conductivity (k)	[W/(m-K)]	Polynomial	Polynomial	Kinetic theory	Kinetic theory
Viscosity	[kg/(m-s)]	Polynomial	Polynomial	Kinetic theory	Kinetic theory
Molecular weight	[kg/kgmol]	FLUENT default	FLUENT default	65.39	81.389
Standard state enthalpy	[J/kgmol]	FLUENT default	FLUENT default	1.304E+08	0
Standard state entropy	[J/(kgmol-K)]	FLUENT default	FLUENT default	160980	43640
Reference temperature	[K]	298.15	298.15	298.15	298.15
L-J Characteristic length	[Angstroms]	FLUENT default	FLUENT default	2.556	2.556
L-J Energy parameter	[K]	FLUENT default	FLUENT default	1356	1356

6 Reaction setting

Reaction setting can be shown in Figure C.5. The properties of gases should be follow

Table C.2.
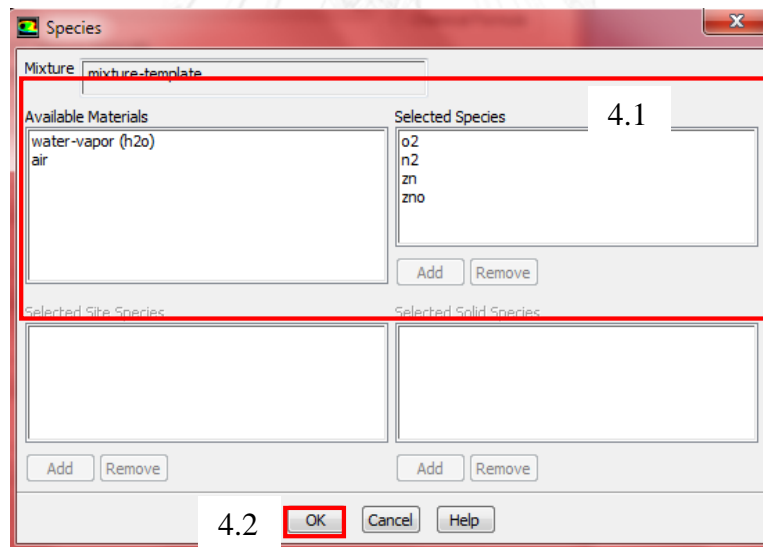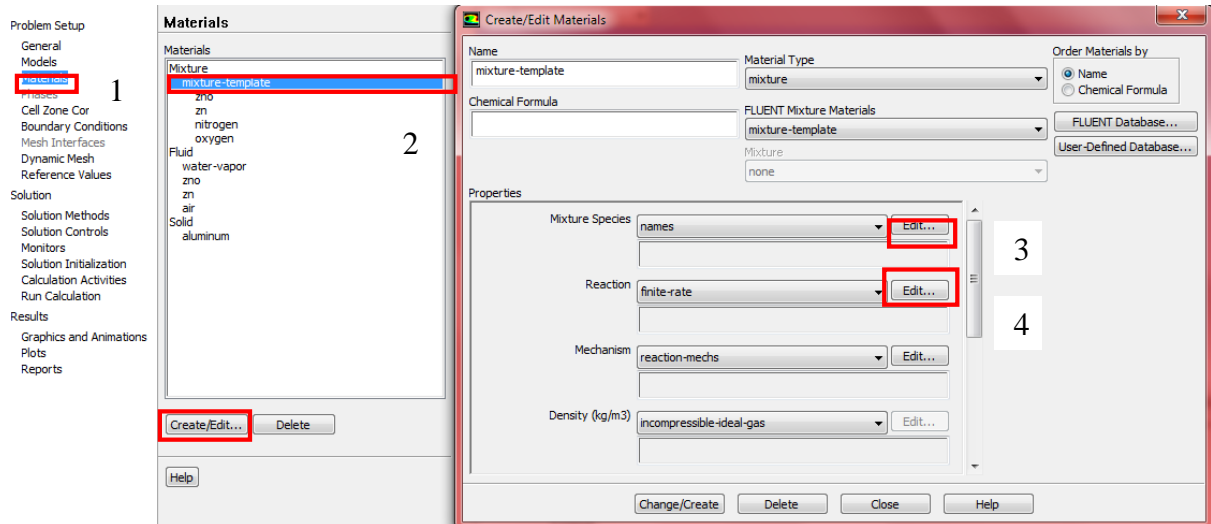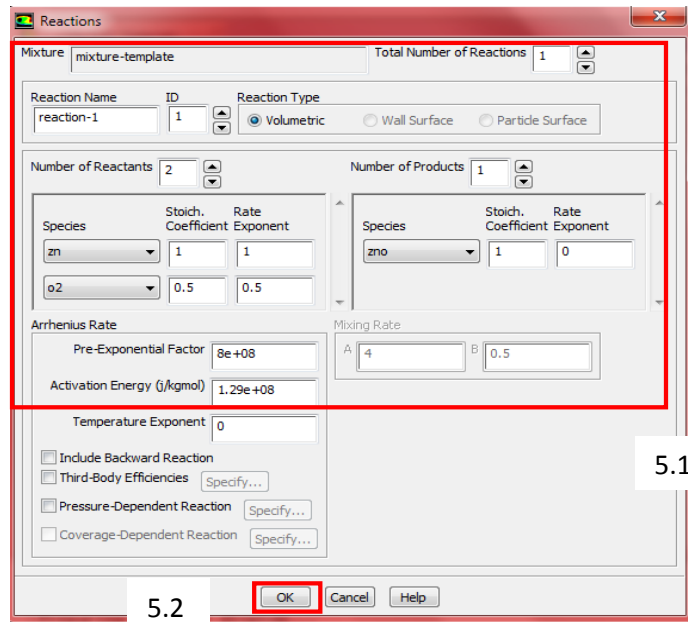
FigureC.5 Reaction setting

$$-r_{Zn} = r_{ZnO} = k_0 [\text{ Zn }][O_2]^{\frac{1}{2}} \tag{1}$$

Reuge et al. employed Eq. (1) for the CFD simulation of ZnO particle formation in parallel flow and cross flow reactors. They adopted the activation energy reported by Garcia et al. and determined the frequency factor as:
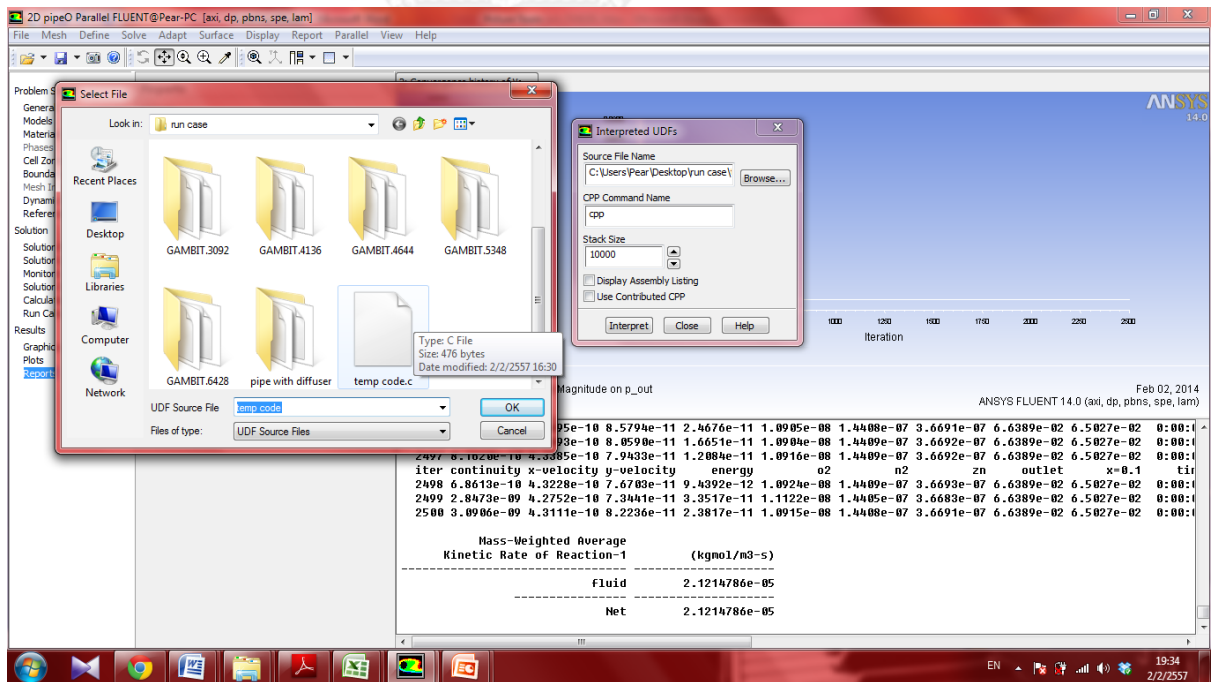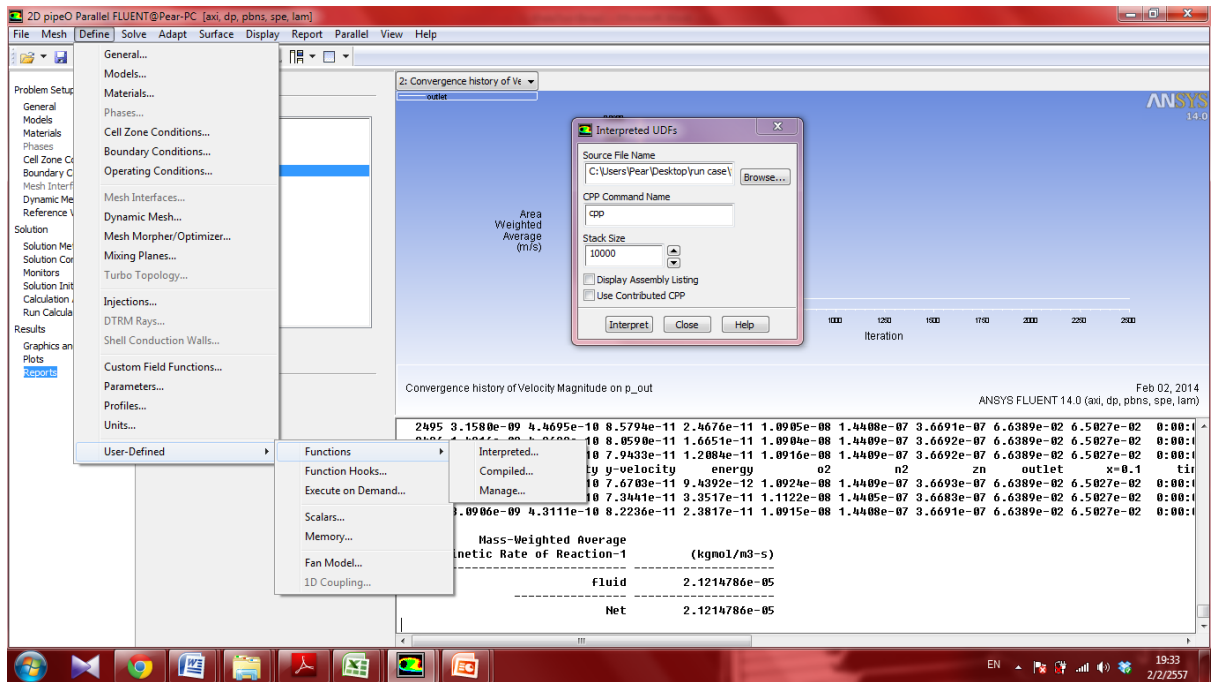
$$k_0 = 8 * 10^8 \exp\left(-\frac{12.9 * 10^7}{RT}\right)$$

7 Boundary condition setting

7.1 Interpreted the C-CODE which is created by Notepad program and save

as.c file (File > save as > type the name.c > save), as shown in Figure

C.6.

The boundary conditions for temperature profile can be written in c-language as the

follow

```c
#include "udf.h"

DEFINE_PROFILE (temp_wall,thread,position)

{

realr[3];

realx;

face_t f1;

begin_f_loop(f1,thread)

{

F_CENTROID (r, f1, thread);

x = r [0];

F_PROFILE (f1, thread, position) = 229049.89*x*x*x*x*x*x - 401566.64*x*x*x*x*x +

255764.26*x*x*x*x - 70248.54*x*x*x + 2711.18*x*x + 2616.07*x + 650.54;

}

end_f_loop(f3,thread)

}
```

7.2 Set the inlet boundary conditions. The inlet boundary condition setting are shown in Figure C.6. The boundary conditions for inlet and outlet are shown in Table C.3.
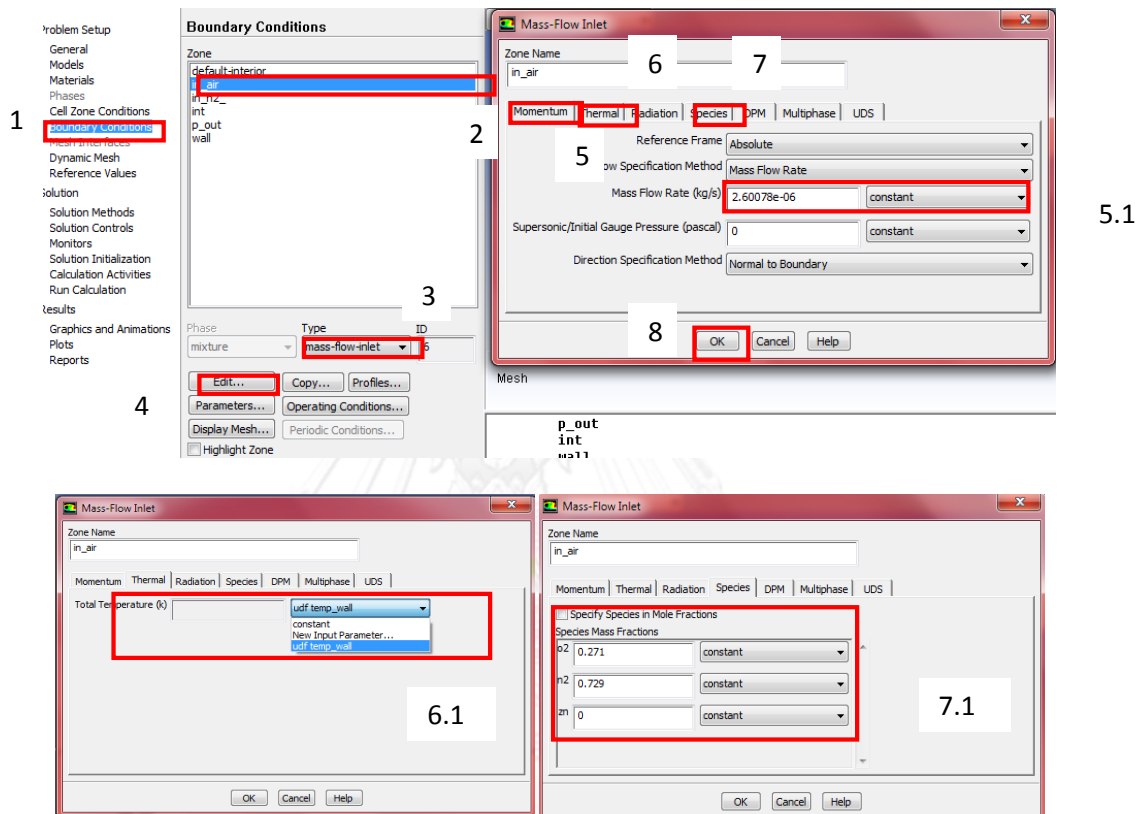

FigureC.6 Inlet boundary conditions setting

TableC.3 Inlet and outlet boundary conditions

Feed	Composition	Reference Temperature	Density	Viscosity	Flow rate		Mass flow rate	Mass fraction
		K	kg/m3	kg/(m-s)	lit/min	m3/s	kg/s	-
Air	N_2	300	1.14	1.66E-05	0.10	1.67E-06	1.90E-06	0.73
	O_2	300	1.30	1.92E-05	0.033	5.42E-07	7.04E-07	0.27
	Total	-	1.18	1.73E-05	0.13	2.21E-06	2.60E-06	1.00
Zn	N2	300	1.14	1.66E-05	2.00	3.33E-05	3.80E-05	0.98
	Zn	300	-	-	-	-	7.40E-07	0.02
	Total	-	-	-	2.00	3.33E-05	3.87E-05	1.00

Feed	Composition	Flow area	Hydraulic diameter	Velocity	Reynolds Number	Note
		m2	m	m/s		
Air	N_2					-
	O_2	0.00064	0.01	0.003	2.34	-
	Total					-
Zn	N_2					-
	Zn	0.00071	0.03	0.047	96.81	0.004 kg
	Total					-

7.3 Set outlet boundary condition. This step likes the previous step.

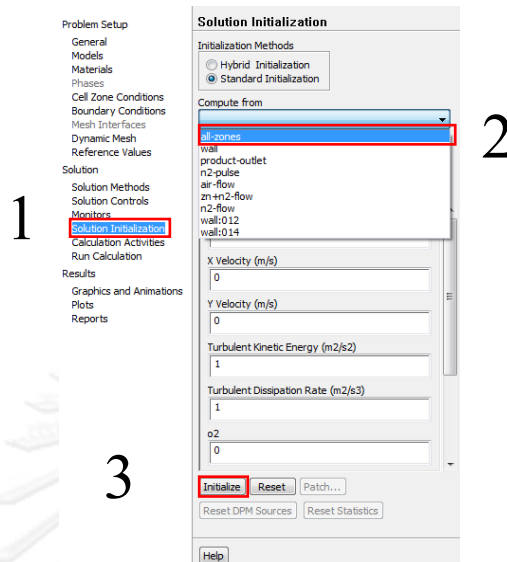7.4 Set wall boundary condition is No-slip

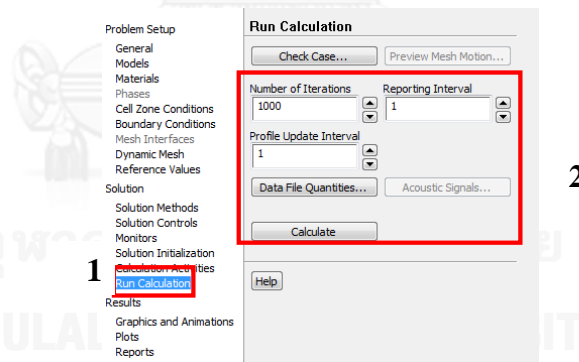7.5 Solution Methods setting. Solution methods setting is shown in

Figure C.7.
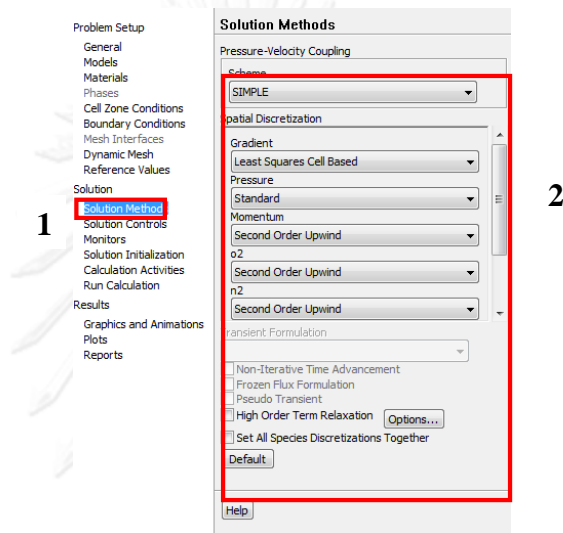
FigureC.7 Solution Methods setting
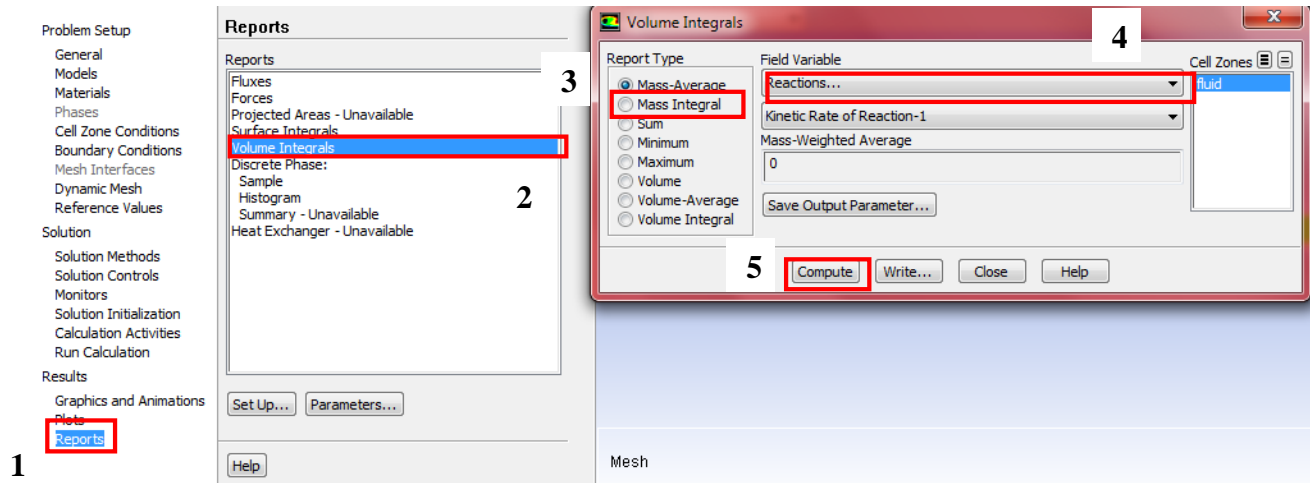
7.6 Solution initialization setting.

FigureC.8 Solution initialization setting

7.7 Run Calculation

FigureC.9 Run Calculation setting

8 How to calculate yields

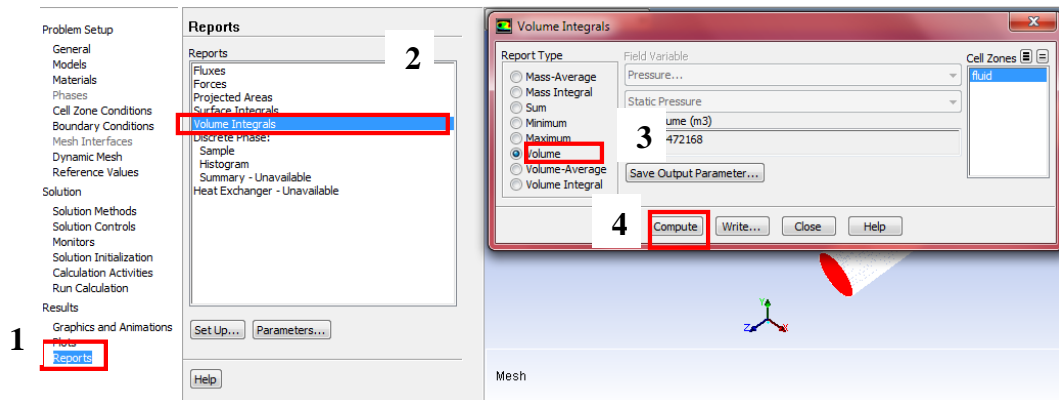FigureC.10 Kinetic Rate of Reaction Calculation setting

Kinetic Rate of Reaction-1 (kgmol/m3-s)

Net   2.4970346e-05

Time operate: 5400 s

Molecular wigth of ZnO: 81.389 kg/kmol

Total volume: 0.0004472 m3

FigureC .11 Total volume Calculation setting

Total mass of ZnO: Kinetic Rate of Reaction x Time operate x Total volume x

Molecular weight : (2.4970346e-05) (5400) (0.0004472)(81.389) = 4.19 kg

VITA

Miss. Passaporn Mahapholsirikul was born on August 23, 1988, in Bangkok, Thailand. She received a Bachelor's degree from the department of Chemical Technology in May 2010 from Chulalongkorn University. After that, She continued to study in Master degree in Center of Excellence in Particle Technology at Department of Chemical Engineering, Faculty of Engineering, Chulalongkorn University.

In May 2014, she participated in Petromt and PPC Symposium 2014, Bangkok, Thailand for proceeding published in "2D CFD simulation of ZnO nanoparticle synthesis using modified French method in tubular reactor